HYDRAULIC TRANSPORT OF SAND AND LIME SLURRIES IN A VERTICAL PIPELINE

by

BRIAN L. JOEL, B.Sc.

A Thesis

Submitted to the Faculty of Graduate Studies

in Partial Fulfilment of the Requirements

for the Degree

Master of Engineering

McMaster University

September 1980

HYDRAULIC TRANSPORT OF SAND AND LIME SLURRIES IN A VERTICAL PIPELINE

MASTER OF ENGINEERING (1980)
Mechanical Engineering

McMaster University
Hamilton, Ontario

TITLE: Hydraulic Transport of Sand and Lime Slurries in a Vertical Pipeline

AUTHOR: Brian L. Joel, B.Sc. (University of the West Indies)

SUPERVISOR: Dr. Brian Latto

NUMBER OF PAGES: xviii, 104

ABSTRACT

This thesis is primarily concerned with the energy required to hydraulically transport sand and lime slurries in a 5.1 cm.-diameter vertical pipeline for both steady and pulsating flows.

In the steady flow experiments, three different grades of sand of average weighted diameter d = 0.66, 1.20 and 1.84 mm. were investigated. The lime slurry used had an average particle diameter of 1.8×10^{-3} mm. The delivered volumetric concentration C_s, the average mixture flow rate Q, and the pressure difference ΔP across the test section were measured within the Reynolds number range of 4×10^4 to 2×10^5.

In the pulsating flow experiments, only one grade of sand of average weighted diameter d = 1.20 mm. was investigated at frequencies of 0.22 and 0.44 cycles per second.

Two methods of predicting pressure gradient for slurry flow were attempted. The first was adapted from Newitt et. al. (1961). By comparing the measured pressure gradient i for various suspensions to those for water flowing under similar conditions i_w, an excess dimensionless pressure parameter ϕ was obtained. It was possible to correlate the steady flow data using ϕ and another dimensionless parameter ψ related to mixture velocity $\overline{V}_m$, diameter ratio $\frac{D}{d}$ and specific gravity of solid S. In the second method the excess pressure gradient (i-iw)

is equated to the excess hydraulic head $C_T(S-1)$. The results are presented in graphical form and each method is appraised in the discussion.

The energy dissipated per unit height of the test section and mass flow rate was determined for steady and pulsating flow of suspensions. The energy ratio J_p/J_s at the two frequencies was obtained for low concentration slurries ($C_S < 8.0\%$). It was found that no energy savings were recorded for pulsatile flow under these conditions.

ACKNOWLEDGEMENTS

The author wishes to express his thanks to Dr. B. Latto under whose guidance and expert advice this research was carried out and who gave generously of his time and experience throughout the course of this program.

Thanks are also extended to those members of the Mechanical Engineering Department who assisted in the successful completion of this program and to Ms. L. Hunter for a splendid job in typing the manuscript.

The studies were co-sponsored by the CCSFA-AUCC and the Government of Trinidad and Tobago to whom the author is extremely grateful.

TO MY PARENTS

TABLE OF CONTENTS

NOMENCLATURE

A	amplitude
C	concentration
C_d	drag coefficient
C_m	delivered mass concentration
C_s	delivered volumetric concentration
C_T	transport volumetric concentration
d	average weighted diameter of solid particles
D	pipe internal diameter
f	friction factor
f_u	friction factor in unsteady flow
f_s	friction factor in steady flow
g	acceleration due to gravity
h	height (or specific pressure head)
h_L	specific pressure head eq. (D-1)
ΔH_m	manometer reading
i	dimensionless pressure gradient, $\Delta P / \rho_w \Delta Z$
i_T	dimensionless pressure gradient including hydraulic head, $\frac{\Delta P_T}{\rho_w \Delta Z}$
i_w	dimensionless pressure gradient for water flowing alone at velocity $\overline{V}_m$, $\left(\frac{\Delta P}{\rho_w \Delta Z}\right)_W$
$\overline{J}_L$	time-averaged rate of energy dissipation Eq. (3-11)

J_o	Bessel function of the first kind
J_p	pulsating-flow energy requirement defined by Eq. (A-13)
J_s	steady-flow energy requirement defined by Eq. (A-9)
K	constant in Eq. (3-2)
M_o	modulus of Bessel function of zero order
$\dot{m}$	mass flow rate
n	number of intervals Eq. (A-13)
P	pressure
ΔP	pressure drop over length ΔZ as seen by manometer
ΔP_{fm}	pressure drop due to friction for mixture
ΔP_{fw}	pressure drop due to friction for water flowing alone
ΔP_T	total pressure drop over length ΔZ
Q	volume rate of flow
Q_L	volume rate of flow for liquid only Eq. (6-1)
r	radial distance
R	internal pipe radius
Re	Reynolds number = $\frac{DV\rho}{\mu}$
S	specific gravity
St	Stokes number = $\left(\frac{\nu}{\omega d^2}\right)^{1/2}$
t	time
T_{amb}	ambient temperature
T_{res}	reservoir temperature
u	local axial velocity
$\bar{u}$	average flow velocity

u_f	fluid average velocity
u_m	mixture velocity
u_o	velocity amplitude Eq. (3-5)
u_p	particle velocity
u_s	steady flow velocity component
U	maximum velocity in flow profile
v	volume of delivered mixture sample
V	velocity
V_L	liquid velocity
$\overline{V}_m$	average mixture velocity
V_o	terminal settling velocity of solids at low concentration
V_{SL}	superficial liquid velocity defined by Eq. (6-1)
W	weight of delivered mixture sample
ΔZ	length of test section

GREEK LETTERS

α	dimensionless frequency dependent parameter = $R\sqrt{\frac{\omega}{\nu}}$
γ	specific weight = ρg
δ	thickness of the lubricating layer Eq. (3-11)
θ_o	phase angle of Bessel function of zero order
μ	viscosity
μ_{wr}	viscosity of water at reservoir temperature
ν	kinematic viscosity = $\frac{\mu}{\rho}$
ρ	density

ρ_f	fluid density
ρ_{Hg}	density of mercury
ρ_l	liquid density
ρ_{mr}	mixture density Eq. (A-6)
ρ_p	particle density
ρ_{wa}	density of water at ambient temperature
ρ_{wr}	density of water at reservoir temperature
τ_o	wall shear stress
ϕ	dimensionless parameter = $\frac{i-i_w}{c_s i_w}$
ϕ (r)	phase shift
χ	added mass coefficient Eq. (3-7)
ψ	dimensionless parameter = $\left(\frac{gD}{2V}\right)^{1/2} \cdot \frac{D}{d} \cdot S^2$
ω	frequency

LIST OF FIGURES

LIST OF TABLES

CHAPTER 1

INTRODUCTION

The vertical flow of solid-liquid mixtures in pipelines finds many applications in modern industry. For example, solids have been transported in fluidized systems while performing the function of either catalyst, reactant or heat transfer medium in various types of reactions in the chemical process industries (Frantz, 1962). Also, in direct contact heat exchangers, gradual removal of scale deposits can be achieved with the addition of abrasive solid particles to the flowing liquid (Barton and Fenske, 1970). In this case vertical flow is encountered since there are vertical lift lines from the base of one tower to the top of the next.

Most of the applications concerning vertical solid-liquid flow, however, are related to the mining industry. For instance, hydraulic hoisting of iron ore and coal from deep mines has been proven to be completely reliable, economically superior and safer than conventional hoisting (Harzer, 1974). And yet, despite its apparent practical importance, our ability even to predict the pressure drop in generalized vertical solid-liquid flow is limited.

In the early stages of design of solid transport by pipeline, the tendency was towards the use of high mixture velocities, since at an increased flow rate the pressure drop-velocity relationship for

solid-liquid mixtures are similar to those of liquid flow. Such practices resulted in higher rates of pump and pipeline wear or size degradation in the case of friable solids. Later on, solids were introduced into water flow systems on the discharge side of the pump by means of 'feeders', while the high-pressure pump handled clean water only. Feeders, which are custom built machines mostly encountered in hydraulic hoisting, seriously hampered the overall pumping efficiency. A further improvement, and one that exists to the present day, involves the use of positive displacement pumps which are capable of handling slurries without serious loss of efficiency.

Recent studies and experiments, carried out by Round, Latto and Lau (1976), have indicated that energy savings can be achieved when low frequency pulsations are superposed on the steady flow of solid-liquid suspensions in a horizontal pipeline. It has also been suggested that the ratio of the energies required for this type of pulsatile flow to that of steady flow is a function of the frequency of pulsation. Furthermore, limited results appear to indicate that a minimum energy ratio may be obtained at some 'threshold' frequency.

In this thesis, the results of experiments that were carried out are presented in an effort to fulfil the following objectives:

(a) To obtain experimental data for lime and medium-sized sand-water suspensions flowing in a 5.1 cm-diameter vertical pipeline,

(b) To obtain generalized correlations for pressure gradient at different mixture velocities and concentrations, and,

(c) To verify, in the light of observations made by Round et. al.

(1976) on horizontal slurry transport, whether energy savings can be made possible with vertical pulsatile transport of slurries.

CHAPTER 2

LITERATURE SURVEY

The present knowledge of the vertical transport of solid-liquid mixtures is a result of extensive studies which were initially undertaken in the field of fluidization. Most of these studies were conducted prior to 1945 with the first articles being published around the 1950's. Beyond the fluidized state, however, attention is focussed on the practical aspect of vertical solid transport in pipelines in slurry form.

Of particular interest to our research are the results presented by Newitt, Richardson and Gliddon (1961). In their experiments, Newitt et. al. investigated the effect of particle size, particle density, size distribution, pipe diameter, slurry concentration, and velocity on the hydraulic gradient of flowing slurries. It was noted that the most striking feature of vertical conveying is the almost negligible influence that the larger particles have on the pressure drop. It was also observed that the density of the solid particles had a marked influence. Graphs expressing the relationship for various sand-water mixtures of hydraulic gradient against mixture velocity at different concentrations are shown in Figures (2-1) - (2-4).

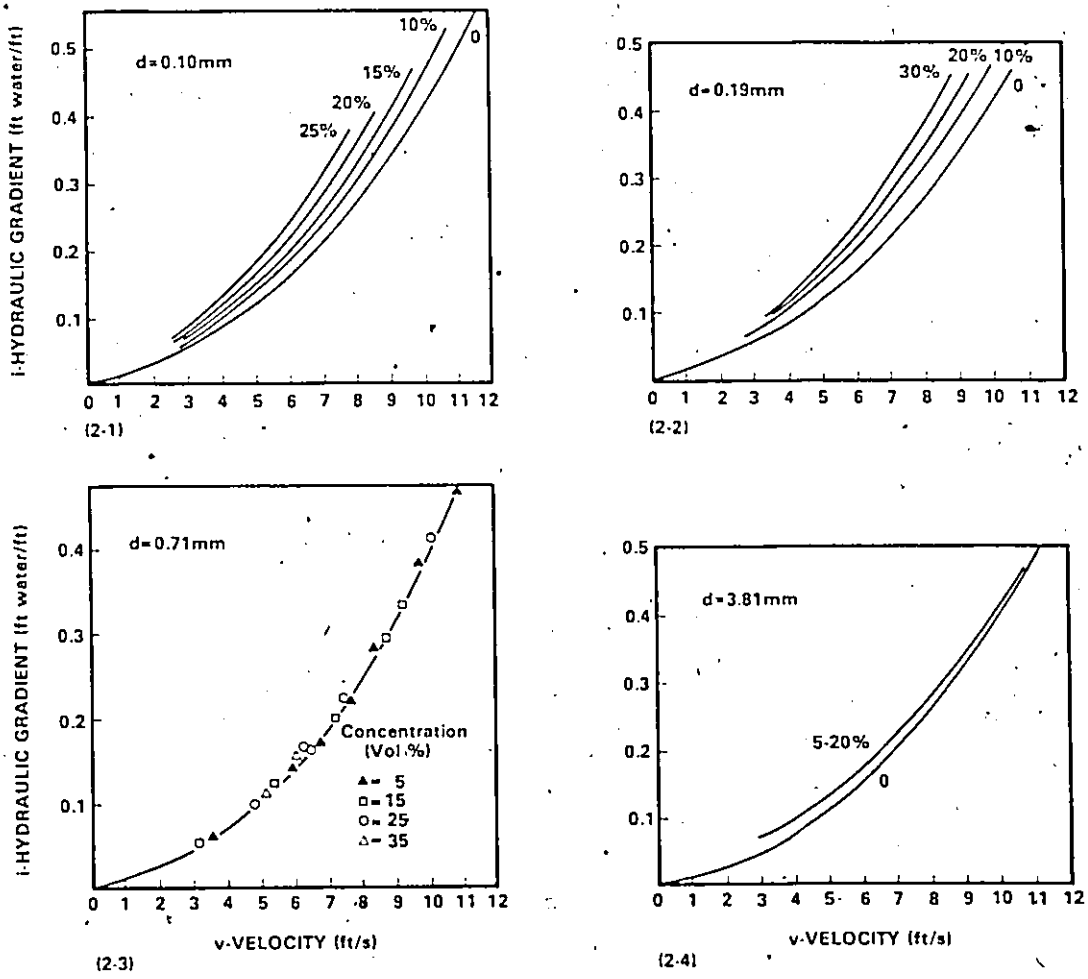

FIGURES (2-1) -(2-4) GRAPHS OF HYDRAULIC GRADIENT AND VELOCITY FOR SAND IN 2.54cm DIAMETER PIPE TAKEN FROM NEWITT et al (1961) THE FIGURES AGAINST THE CURVE INDICATE THE CONCENTRATION (VOL %)

Durand's (1953) experiments with coarse sand particles led him to the conclusion that the pressure drop when a slurry is being conveyed is the same as for water only flowing at the same average velocity, provided allowance is made for the static head of the solids in the pipe.

Including results obtained by Bhattacharya and Roy (1955), Newitt et. al. found that for slurries composed of small particles $d \leq 0.25$ mm the dimensionless parameter, $^{i-i_w}/_{Ci_w}$, can be satisfactorily correlated to the Froude number, $\bar{V}_m^2/gD$, specific gravity, S, and diameter ratio, $^D/_d$, by the following empirical equation:

$$\frac{i-i_w}{Ci_w} = 0.0037 \left(\frac{gD}{\bar{V}_m^2}\right)^{\frac{1}{2}} \left(\frac{D}{d}\right) S^2 \qquad (2.1)$$

Meanwhile, the study of particle motion in oscillating liquids has assumed greater importance within the last thirty years. Houghton (1966) in an attempt to predict the general behaviour of free particles in a sinusoidal velocity field stated that "the dynamic behaviour of particles such as bubbles, droplets and solids particles in an oscillating continuous phase can have a pronounced effect on the holdup and mass or heat transfer characteristics of the resulting two-phase system."

An investigation by Baird, Senior and Thompson (1967) dealt specifically with the quantitative effect which low frequency liquid oscillations or pulsations have upon the average settling velocity of single spherical particles. It was found that such oscillations resulted in a decrease of up to 28 percent in the terminal velocity of

the particles tested. It is also interesting to note that frequency was found to have more of an effect on retardation than amplitude. In correlating the results Baird et. al. obtained the following expression:

$$\frac{u_p}{u_s} = \phi\ (\omega A^{1/3}) \qquad (2.2)$$

(see Figures 2.5 and 2.6).

Molinier and Angelino (1976) working with monochlorobenzene and carbon tetrachloride droplets in water under pulsed conditions found that their results were also well correlated by equation (2-2) (see Figure 2.7).

Edwards and Wilkinson (1971), in extending this concept to pulsating flows, analysed the effect of superposed oscillations on steady flowing solid-liquid suspensions in pipelines. They predicted that there are advantages to be gained in terms of energy requirements when pulsing Newtonian 'settling' suspensions. Limited experimental data by Round, Latto and Lau (1976) suggests that the ratio of pulsating energy to steady flow energy is a function of the frequency of pulsation. Both Round et. al. and Colamussi and Merli (1972) observed that this energy ratio approached a minimum value at some frequency lying between 0 and 0.25 Hz.

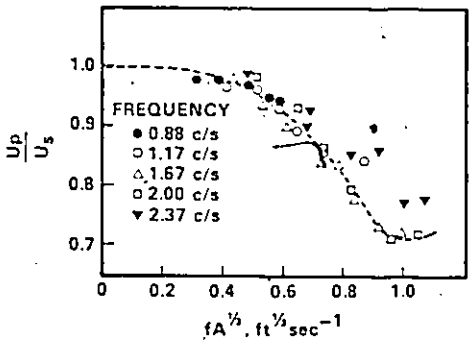

FIG. 2.5. RETARDATION OF 6.35mm DIAMETER PLASTIC SPHERES. (BAIRD M.H.I., SENIOR M.G. AND THOMPSON R.I. CHEM. ENG. SCI., 1967 VOL. 22 P.P. 551-558)

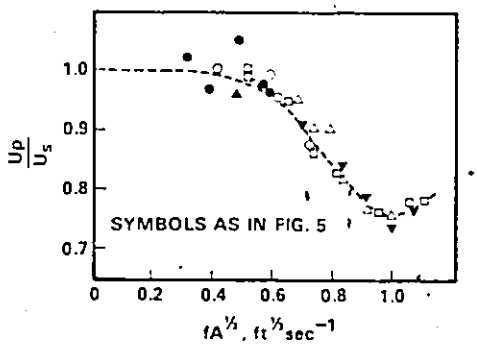

FIG. 2.6 RETARDATION OF 12.7mm DIAMETER PLASTIC SPHERES (BAIRD M.H.I., SENIOR M.G. AND THOMPSON R.I. CHEM. ENG. SCI. 1967 VOL. 22 P.P. 551-558)

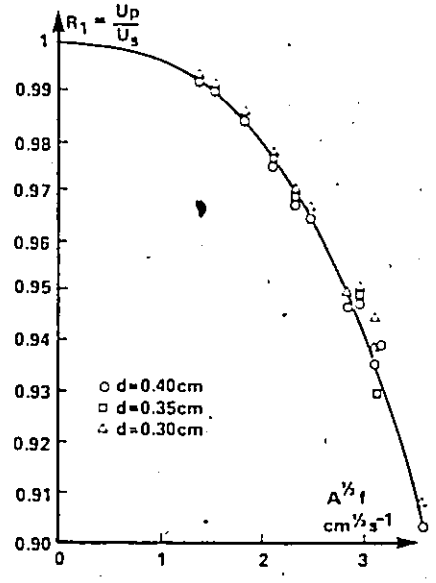

FIG. 2.7 RETARDATION OF MONOCHLOROBENZE AND CARBONTETRACHLORIDE DROPLETS IN WATER (MOLINIER J. AND ANGELIND H. CAN. JOURNAL OF CHEM. ENG. VOL. 54. 1976).

Summary of Literature Review

A list of the vertical flow experiments, which have been carried out with medium-sized solid suspensions, is given in Table (2.1). From these studies, attempts have been made to predict the pressure drop of slurries composed of irregularly-shaped sand and uniformly shaped dense particles. So far, the most successful equation for correlating the data for the hydraulic transport of medium-sized and coarse solids in vertical pipes can be expressed as follows:

$$\frac{\Delta P_T}{\rho_l \Delta Z} = C_T (S-1) + 1 + f \frac{V_l^2}{2gD} \qquad (2.3)$$

Kostuik (1966) has suggested that the application of Equation (2.3) should be limited to the condition given by $V_m/V_o \geq 10$. But apart from this restriction on flow velocity, the researchers listed in Table (2.3) all seem to be in general agreement with this equation. Kopko et. al. (1975) further states that in Equation (2.3) the pressure drop due to solid-solid and solid-wall collisions is considered to be negligible.

However, observations made of hydraulic lifting in transparent tubes by Newitt et. al. (1961) and Toda et. al. (1969) makes it clear that the amount of inter-solids collisions increases with rising size distribution band-widths and decreasing fluid velocities. They claim that smaller particles because of their lower free settling velocities tend to rise faster, colliding with bigger particles. Again, at low fluid velocities and particularly at high concentrations, solid-wall

Table (2-1)

Medium-sized sand-water suspensions tested in vertical flow

Solid Material	d (mm)	D (cm)	S	C	Reference
sand	0.36	10.48	2.60	0.35	Oedjoe et al (1966)
sand	0.38	1.27	2.64	0.60	
sand	0.38	1.90	2.64	0.60	Cloete et al (1967)
glass	0.43	1.27	2.50	0.60	
glass	0.43	1.90	2.50	0.60	
glass	0.44	3.02	2.50	0.10	Toda et al (1969)
sand	0.71	2.54	2.59	0.35	Newitt et al (1961)
glass	0.98	3.02	2.50	0.10	Toda et al (1969)
sand	1.00	15.00	2.60	0.10	Durand (1953)
iron	1.86	6.10	7.59	0.41	Kopko et al (1975)
glass	2.07	3.02	2.50	0.10	Toda et al (1969)
glass	2.78	3.02	2.50	0.10	
iron	3.33	6.10	7.56	0.41	Kopko et al (1975)

collision becomes significant. This latter effect is reduced at higher velocities when a well-defined core of solid particles tend to be formed.

These factors, which are usually overlooked, are mainly responsible for the shortcomings in pressure drop predictions based on Equation (2.3). Reliable results in limited ranges of particle size, sieve rating, concentration, velocity and tube diameter can only now be obtained by carrying out the necessary experiments. This lack of knowledge is more evident in the area of vertical pulsating flow of slurries where no experimental data exists and which forms part of this thesis.

CHAPTER 3

THEORETICAL CONSIDERATIONS

Since a complete theoretical analysis of the vertical flow for solid-liquid mixtures under steady conditions can be found in Govier and Aziz (1972), only pulsating flows will be treated in this chapter.

For a suspension of solid particles in a Newtonian liquid flowing upward in a vertical pipeline under pulsating conditions, there are two main considerations on which a simplified theoretical approach can be based. These considerations are:

(1) The effect which oscillations exert on Newtonian liquids flowing in pipes,

(2) The motion of individual solid particles in oscillating Newtonian liquids.

When combined, the overall behaviour of this ideal model has to be modified in order to represent real pulsatile flow of Newtonian "settling" suspensions. Thus, the main factors which must be accounted for are collision between particles, shape irregularities, the effects of the tube wall and the concentration.

3.1 Oscillating Flow of Newtonian Liquids Through a Pipe

(a) Analysis of Theoretical Model:

A standard approach to the oscillating flow of Newtonian liquids and one described by Schlichting (1968) is given as follows:

Let us consider a very long circular pipe. We shall denote the longitudinal distance in the direction of the flow by x, and the radial distance from the pipe axis by r. Under the assumption that the test section was sufficiently far from the last bend, the flow may be taken as fully developed and independent of x. When the axial velocity component, u, ceases to depend on x, the other velocity component must vanish together with the convective terms parallel to the tube axis. Thus the Navier-Stokes equation assumes the form

$$\frac{\partial u}{\partial t} = -\frac{1}{\rho}\frac{\partial p}{\partial x} + \nu\left(\frac{\partial^2 u}{\partial r^2} + \frac{1}{r}\frac{\partial u}{\partial r}\right), \qquad (3\text{-}1)$$

which is exact as it implies no additional simplifications.

The boundary condition is $u = 0$ for $r = R$ at the wall. It shall be assumed that the pressure gradient caused by the motion of a piston is harmonic and is given by

$$-\frac{1}{\rho}\frac{\partial p}{\partial x} = K \cos \omega t \quad , \qquad (3\text{-}2)$$

where K denotes a constant. It is convenient to use complex notation

to express the L.H.S. of equation (3-2), that is

$$-\frac{1}{\rho}\frac{\partial p}{\partial x} = K\, e^{i\omega t}$$

and attribute physical significance only to the real part.

Assuming that the velocity function has the form $u(r,t) = f(r)\, e^{i\omega t}$, and referring to eqn. (3-1), we obtain the following differential equation for the function $f(r)$:

$$f''(r) + \frac{1}{r} f'(r) - \frac{i\omega}{\nu} f(r) = \frac{K}{\nu}$$

the solution of which is

$$u(r,t) = -i\frac{K}{\omega} e^{i\omega t}\left\{1 - \frac{J_o\left(r\sqrt{\frac{-i\omega}{\nu}}\right)}{J_o\left(R\sqrt{\frac{-i\omega}{\nu}}\right)}\right\} \qquad (3\text{-}3)$$

Here J_o denotes the Bessel function of the first kind and of zero order.

Remembering that $-1 = i^2$, expressing r/R as y and defining α as a dimensionless frequency dependent parameter given by the quantity $R\sqrt{\frac{\omega}{\nu}}$, the solution may be written as:

$$u(r,t) = +\frac{K}{i\omega} e^{i\omega t}\left\{1 - \frac{J_o\left(\alpha\, y\, i^{3/2}\right)}{J_o\left(\alpha\, i^{3/2}\right)}\right\} \qquad (3\text{-}4)$$

(b) Interpretation Of Solution

Womersley (1955) made use of tables provided by McLachlan

(1941) for the Bessel Functions in eqn. (3-4) in the form:

$$J_o\ (x\ i^{3/2}) \quad = \quad M_o(x)\ e^{i\theta_o(x)}$$

He also assumed that the velocity at any point in the tube is a function of time and varies in a periodic manner similar to the pressure gradient. However, the velocity will not be in phase with the applied pressure gradient and can be expressed as:

$$u\ (r,t) \quad = \quad U_o(r)\ [\cos\ \omega t + \phi(r)] \qquad (3\text{-}5)$$

where, $U_o(r) \quad = \quad \frac{K}{\omega}\ (1 + h_o^{\,2} - 2\ h_o\ \cos\ \psi)^{1/2}$,

and, $\phi(r) \quad = \quad \tan^{-1}\ [h_o\ \sin\ \psi\ /\ (1 - h_o\ \cos\ \psi)]$,

such that,

$$h_o \quad = \quad M_o\ (\alpha y)\ /\ M_o\ (\alpha)$$

$$\psi \quad = \quad \theta_o\ (\alpha) - \theta_o\ (\alpha y)$$

Edwards and Wilkinson (1971) stated that, by separating eqn. (3-4) into its real and imaginary parts, the velocity amplitude, $U_o(r)$, can be found as a function of y and the frequency dependent parameter α. If this is done it will be found that at low frequencies the amplitude of the velocity is nearly parabolic with a maximum at

the tube axis. At the higher frequencies, however, the maximum occurs between the axis and the wall and this peak moves towards the wall as the frequencies increase. Fig. (3-1) shows this effect.

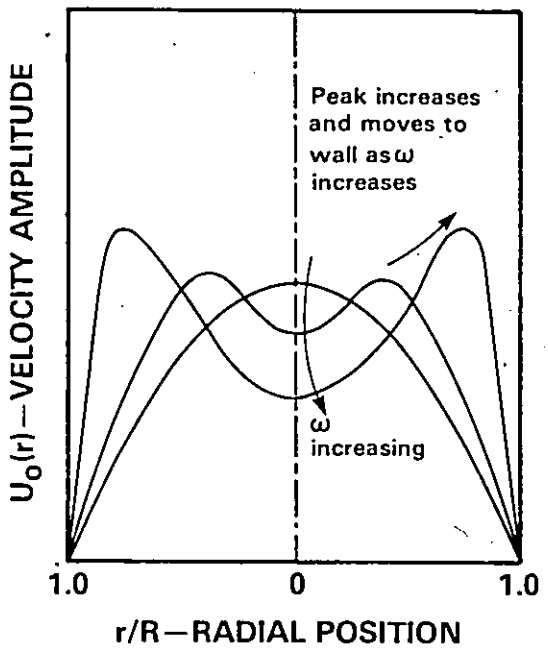

Fig. (3-1). Effect of frequency upon velocity amplitude (after Edwards et. al. (1971)).

(c) Effect on Shear Rate

There seems to be, at present, no rigorous theoretical approach for the comparison of the shearing rate of steady and unsteady flows in pipes. Carstens and Roller (1959) hypothesized that the velocity distribution is similar for both steady and unsteady flow at moderate accelerations. They then formulated the following expression for

the boundary drag coefficient ratio,

$$f_{u/f_s} = 1 + 0.449 \, D/f_s u_m^2 \, \frac{du_m}{dt} \qquad (3\text{-}6)$$

where, $f = 8 \tau_o / \rho u_m^2$

τ_o = wall shear stress

Also, from their results they concluded that for turbulent flows in pipes eqn. (3-6) approaches $f_{u/f_s} = 1$.

Using a similar assumption, Edwards et. al. (1971) deduced, that with Newtonian fluids in pulsating flows, there is no increase in the mean delivery rate, $\bar{Q}$, and extra power is required to maintain the pulsations. As a further consideration, a more likely qualitative analysis was proposed in the latter paper to account for the shearing phenomenon in unsteady flow.

It states that, with highly viscous materials, the energy dissipation, resulting in shear heating, can be appreciable since it depends upon the square of the shear rate, $\mu(\partial u/\partial r)^2$. When pulsating flow is superimposed on steady flow the mean shear rate is greatly increased in a region close to the wall. With viscous, poorly conducting materials this could give rise to a high temperature layer near the wall due to the shear heating. If the viscosity is sensitive to temperature, as it is for many viscous materials, the

effect would be to set up a low viscosity layer near the wall which would act as a lubricant for the main core of the flow in much the same way as appears likely for thixotropic fluids. Again the input of energy to maintain pulsating conditions could result in a reduction of total pumping power.

3.2 Motion of Small Spheres in Oscillating Liquids

Herringe (1976) revised several papers on the motion of small spheres in oscillating liquids. Thus he realized that the basic analytical approaches of Houghton (1962, 1966, 1968), Molinier et. al. (1971), Chonowski and Angelino (1972), Baird et. al. (1967), Ho (1964) and Field (1968) stem from the equation for the unsteady motion of a sphere initially derived by Basset (1888) for a stationary fluid and later by Tchen (1959) for a moving fluid. In developing the theoretical model it was realised that the force opposing motion is composed of three separate terms: the steady state drag expression, the added mass term to account for the fact that the fluid must also be accelerated around the particle, and the history term which is necessary because the particle is entering a region in which the fluid flow pattern has been affected by previous particle movement. This relation may be written as:

$$T_1 = T_2 + T_3 + T_4 + T_5 + T_6 \qquad (3\text{-}7)$$

where T_1 is the mass-acceleration product of the particle,

$$T_1 = \frac{\pi d^3}{6} \rho_p \frac{du_p}{dt}$$

T_2 is the Stokes linear drag force,

$$T_2 = -3\pi\mu d(u_p - u_f)$$

T_3 is the force resulting from the pressure gradient in the accelerating fluid,

$$T_3 = \frac{\pi d^3}{6} \rho_f \frac{du_f}{dt}$$

T_4 is the added mass term, describing the exchange of energy with the fluid,

$$T_4 = \chi \frac{\pi d^3}{6} \rho_f \left(\frac{du_f}{dt} - \frac{du_p}{dt} \right)$$

T_5 is the net buoyancy force on the particle,

$$T_5 = \frac{\pi d^3}{6} (\rho_f - \rho_p) g$$

and T_6 is the history term, taking into account the deviation of the flow pattern from steady state conditions,

$$T_6 = 3/2\, d^2\, (\pi \mu \rho_f)^{1/2} \int_{t_o}^{t} (t-t')^{-1/2} \left(\frac{du_f}{dt'} - \frac{du_p}{dt'} \right) dt'$$

The coefficient χ preceding the term T_4 is usually referred to as the added mass coefficient and is usually given a value of 0.5.

The complete eqn. (3-7) applies for low Reynolds number (Re < 0.1) particles through oscillating fluids, simple averaging tells us that the mean fall velocity, $\bar{u}$, will be identical to the equivalent steady state velocity. The complete motion of a particle can be represented by an amplitude ratio and a phase lag of the particle motion with regard to the fluid motion and it was shown by Hjelmfelt and Mockros (1966) that these two variables are unique functions of the density ratio (particle-to-fluid) and a Stokes number defined as:

$$St = (\nu/\omega d^2)^{1/2}.$$

For higher Reynolds numbers, eqn. (3-7) will no longer apply since it has been observed that in these situations particles fall at velocities lower than their equivalent steady state values. Houghton (1963) suggested that the Stokes linear drag term should be replaced by the equivalent steady state expression for higher Reynolds number, i.e.

$$T_2 = -C_d \frac{1}{2} \rho_f \frac{\pi d^2}{4} (u_p - u_f)(u_p - u_f) \qquad (3\text{-}8)$$

so that the equation of motion would then be:

$$T_1 = \left(-C_d \frac{1}{2} \rho_f \frac{\pi d^2}{4} (u_p - u_f) \quad (u_p - u_f)\right) + T_3 + T_4 + T_5 + T_6 \qquad (3\text{-}9)$$

Houghton further suggested that the history term could be neglected and he solved eqn. (3-9) with T_6 equal to zero and with the value of C_d equal to a constant value based on the steady state terminal velocity of the particles. Tunstall and Houghton (1968) tested Houghton's analysis experimentally and found that smaller particles fell faster than predicted while larger particles fell slower. A more realistic approach would be to base the value of the drag coefficient on the instantaneous relative velocity rather than on the constant steady state value suggested by Houghton. Ho (1964) found that by this method predictions of mean velocity were much more reliable than those reported by Houghton, although the larger spheres ($d > 1.5$ mm) still fell significantly more slowly than predicted.

Herringe concluded that (for other than purely viscous conditions) none of the analytical treatments so far adequately describes the motion of particles falling through oscillating liquids. Study of available data indicates that the discrepancy between theory and experiment stems from the arbitrary replacement of the Stokes linear drag expression in the equation of motion by the equivalent steady state expression for higher Reynolds numbers. He suggests that a more correct drag expression may be obtained if the occurrence of vortex shedding is more closely analysed.

3.3 Pulsating Slurry Flows in Pipelines

Shizgal et. al. (1965) observed that a particle-free layer developed after oscillation for about 5 minutes in oscillating polystyrene sphere-water suspensions containing 5-20% by volume of solids. If steady flow was established with a 20% suspension, then a flow situation developed in which a central core of solids moved as a plug on a lubricating layer of particle-free liquid. This is illustrated in Fig. (3-2):

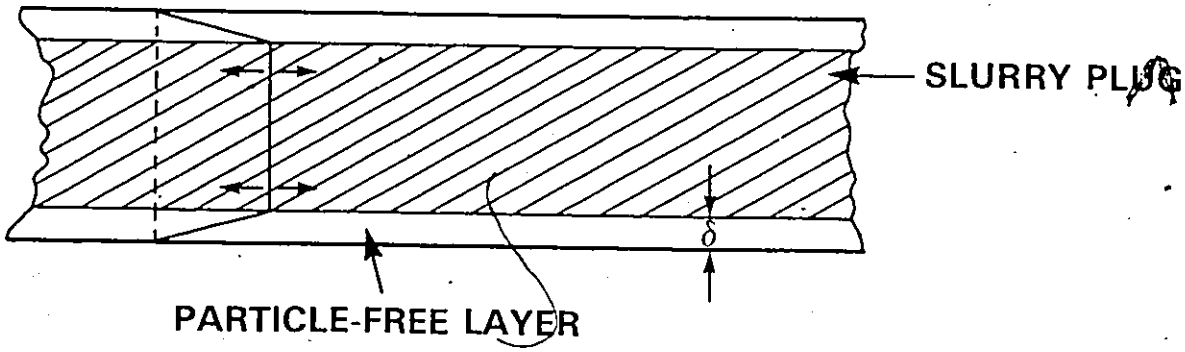

Fig. (3-2). Pulsating flow of slurries of high volumetric concentration (after Edwards and Wilkinson)

The velocity of the plug was given by Shizgal et. al. as

$$u = u_s + U_o e^{i(\omega t + \phi)} \qquad (3\text{-}10)$$

with the energy consumption per unit length evaluated as the sum of the steady flow and oscillatory components averaged over one cycle as:

$$\overline{J_L} = \frac{2\pi R\mu}{\delta} \left(u_s^2 + 1/2\ U_o^2\right) \qquad (3\text{-}11)$$

where δ = thickness of the lubricating layer.

It has been pointed out by Edwards and Wilkinson that the second term in the energy equation, although producing no net flow, can increase the particle-free layer thickness and since the energy requirement is inversely proportional to this particle-free layer it is possible to cause a net reduction in the energy for a given flow rate.

CHAPTER 4

DESCRIPTION OF APPARATUS

The general arrangement and flow diagram of the experimental apparatus is shown in Figure (4-1).

4.1 Flow Circuit: The flow circuit consisted mainly of a vertical loop of 5 cm.-diameter standard steel pipe approximately 21.3 m. long. In order to achieve upward vertical flow, the pipeline was first directed downwards for a length of 4.0 m., then there was a large U-bend with a radius of curvature of 58 cm. made of 3.8 cm.-diameter standard steel pipe and finally a 7.6 m. vertical section of 5.1 cm.-diameter standard pipe. The test section was attached to the top end of the latter section. After leaving the test section, the fluid was returned to a 132 litre-reservoir tank for recirculation.

4.2 Pumping Unit: Circulation of the sand-water mixtures was achieved by a Moyno progressing cavity pump type CDQ, frame 3L8, coupled to a 14.9 KW, 1160 R.P.M. Brook electric motor via a 31.7 cm OD. Lovejoy 3225 variable speed pulley drive with a speed ratio of 3:1. Three 7 cm.-wide flat belt pulley sheaves were used on the pump with outside diameters of 35, 50 and 60 cm. respectively to accommodate ribbed V-belts. In order to maintain proper belt tensions and vary

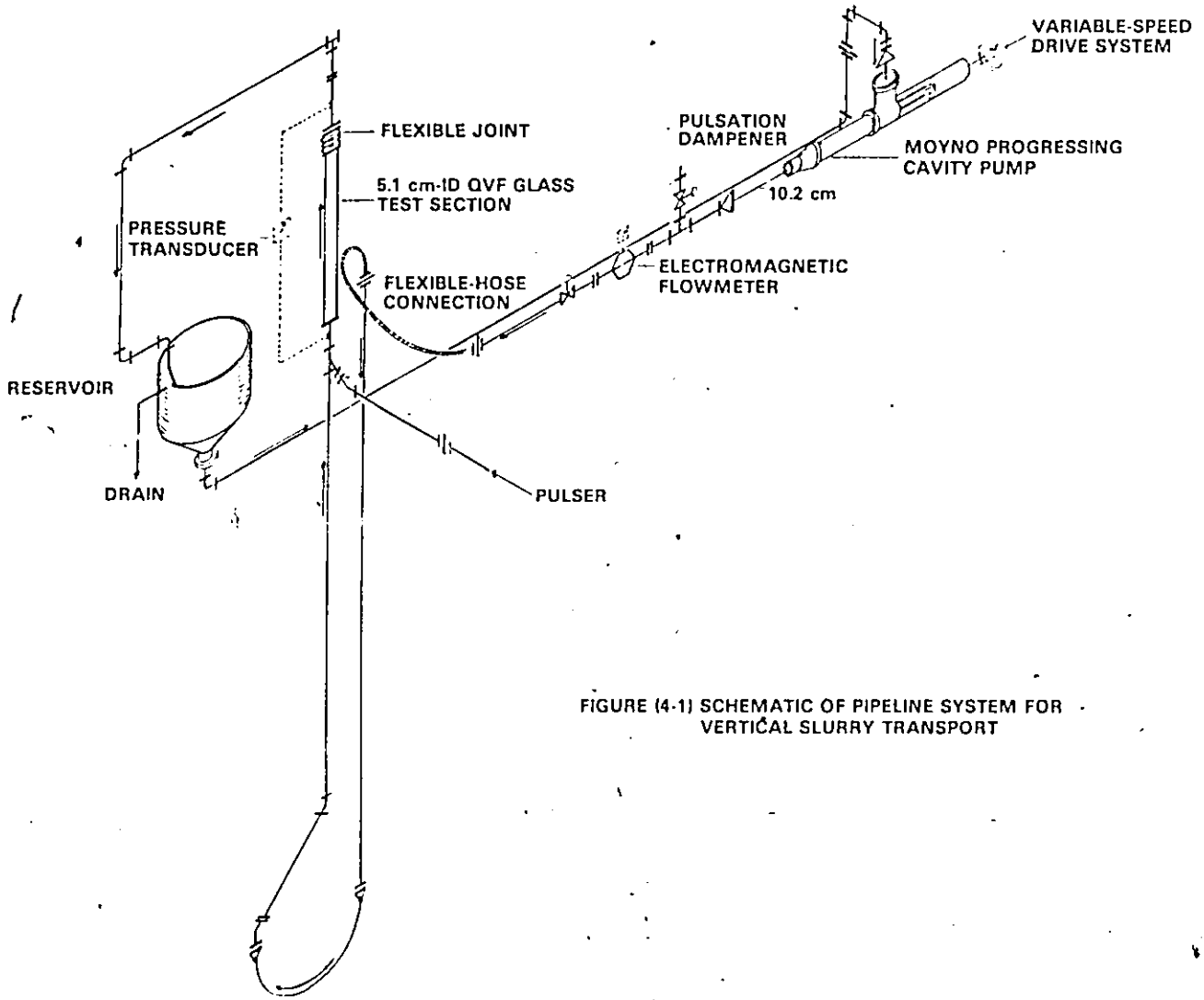

FIGURE (4-1) SCHEMATIC OF PIPELINE SYSTEM FOR VERTICAL SLURRY TRANSPORT

pump speeds, an adjustable motor base was used. With this configuration the maximum pump speed attained was 900 R.P.M. The corresponding maximum flow rate, flow velocity and Reynolds number in the pipeline were 440 litres per minute, 3.1 m/sec. and 1.4×10^5 respectively.

4.3 Test Section: The test section had an overall height of 2.22 m. and consisted mainly of a 1.8 m. long 5 cm. I.D., Q.V.F. glass tube. The glass tube was flanged directly to the steel pipe at one end and to a flexible, expansion joint at the other so that it was protected against misalignment and excessive vibration. Two 0.635 cm.-diameter pressure taps marked the extremities of the test section. The measured average diameter of the test section was 5.1 cm.

4.4 Pulser Mechanism: Pulsed flow was created by means of a variable stroke reciprocating piston device as shown in schematic diagrams Figures (4-2) and (4-3).

Basically, the pulser consisted of a linkage mechanism whereby the rotation of a 25.4 cm.-diameter steel crankwheel, mounted on a 1.9 cm.-diameter crankshaft, created a reciprocating motion on a piston at the end of an aluminum connecting rod. The piston was made of three layers of 1.9 cm.-thick plywood machined to 14 cm.-diameter. A 1.1 cm.-diameter brass fitting inserted into a hole on one side of the piston face formed the priming port. The piston was firmly clamped at one end of a chamber made of 15.2 cm. ID collapsible bellows type tubing. The tubing was composed of double ply neoprene impregnated cotton, spiral wound and supported by rust resistant helical steel

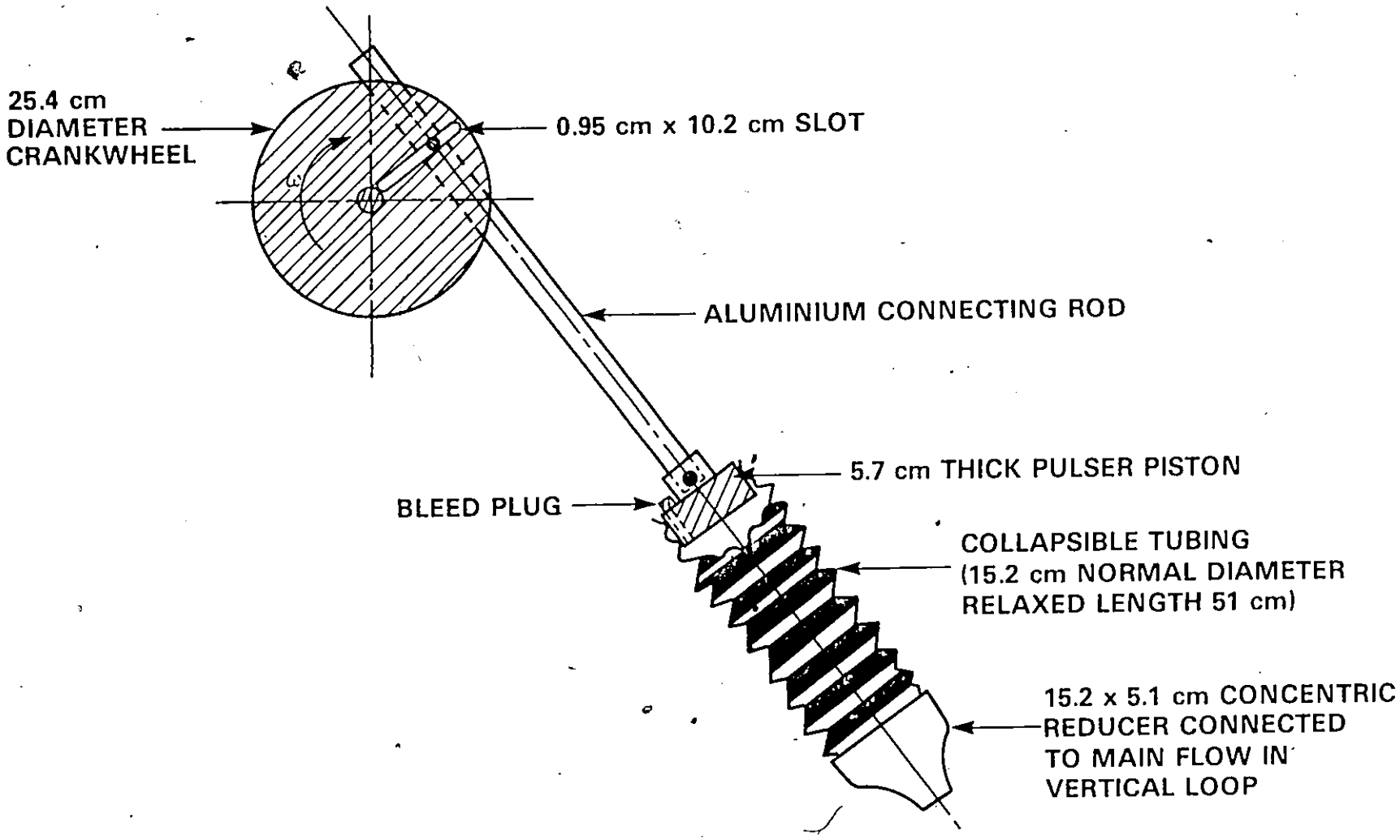

FIGURE (4-2) SKETCH OF LINKAGE MECHANISM (not to scale)

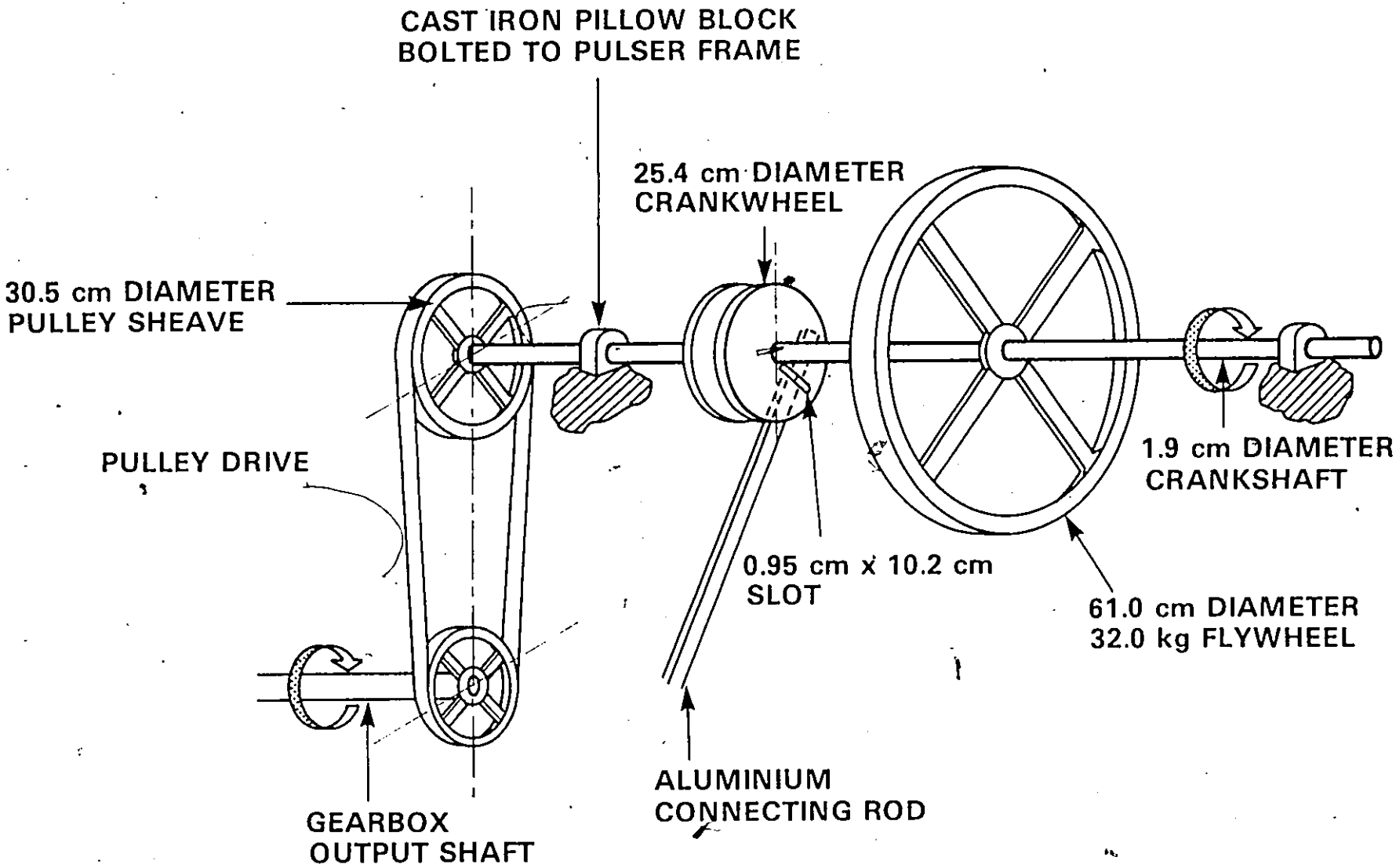

FIGURE (4-3) SKETCH OF PULSER DRIVE MECHANISM (not to scale)

wire. The other end of the chamber was again held by a hose clamp tightened around a 15.2 cm x 5.1 cm. concentric reducer with a 8.9 cm long extension made of 14 cm. OD steel pipe. A liberal amount of silicon rubber cement was applied to the surfaces to which the collapsible tubing was to be attached before the clamps were tightened. This provided additional adhesive strength and formed a waterproof seal around the tubing. The overall effect, created by rotation of the crankshaft, was an accordian-type motion of the collapsible tubing which was filled with the sand-water suspension. The maximum stroke length was 22 cm. such that the corresponding flow pulse was 1.7 litres per stroke. The main stream of flow was pulsed through the side arm of a 5 cm. Y-lateral installed before the test section. A length of 1.2 m. of 5 cm. standard steel pipe connected the reducer to the Y-lateral.

The crank mechanism was driven by a 3.7 KW, 1800 RPM Lincoln electric motor coupled to a Boston worm gear reductor model 332-A, 30:1, 1.85 KW. The rotational speed of the crankshaft was varied by employing a pulley drive. The crankshaft pulley sheave was 1.3 cm. wide, 30.5 cm. diameter while the reductor output shaft was fitted with sheaves of diameters 8.6 cm., 15.2 cm.

The corresponding pulsation frequencies developed were 0.22, and 0.44 cycles per second respectively.

4.5 Instrumentation and Miscellaneous Devices: The flowrate was measured using a Brooks-Mag Electromagnetic flowmeter model 7100/7200 with a maximum measurement capacity of 784 litres per minute. The

flowmeter consisted essentially of a flowhead which provided an electromagnetic field for the generation of an a.c. output signal by the liquid conductor proportional to the flow rate. This signal was amplified and converted into a d.c. signal by a Brooks model 7300 signal converter. The d.c. signal was represented as a percent of the maximum flow on the converter indicator.

Pump speed was measured with a Strobotac type 1531 stroboscope. Pump generated 'noise' was reduced by a pulsation dampener which consisted of an upright cylindrical steel tank 1.5 m. high and 46 cm. in diameter. This tank was partially filled with water and with pressurized air above the water. Pressure fluctuations in the system were resisted due to the compressible nature of the air. The use of this device was limited to steady flow experiments.

The pressure drop across the test section was measured with a Pace model P7D transducer and model CD-25 indicator. The instantaneous pressure drop and flow rate signals were registered on a Rikadenki model B-281L two-pen recorder.

CHAPTER 5

EXPERIMENTAL PROCEDURE

5.1 Preparation

a) The Flow System: The reservoir was filled with cold mains water until the level had reached the overflow mark. The valves in the flow circuit were then fully opened to ensure a low start-up pressure in the system. The pump was started with the exit flow directed into the overflow tank. When the water level in the reservoir dropped to one quarter full, the pump was switched off and the water level allowed to rise once more. This process of flushing the system was repeated until the water in the test section became clear and free of solid particles. With the flow redirected for water circulation, and the pump left running, the flow was allowed to stabilize and air bubbles removed. It became necessary to record the reservoir water temperature for each run, since the mains water temperature varied from 5 to 8^{o}C, and circulation through the pump caused the water temperature in the flow circuit to increase.

b) The Measurement Systems: The flowmeter and transducer indicators were switched on prior to experimental runs to allow them to warm up. The bleed ports of the transducer were opened so that

water flowed through the pressure tap lines until no more air was trapped in the lines. Then the terminals from the flowmeter and transducer indicators were connected to the two-pen recorder. Care was taken that the indicators were set to zero at no flow conditions.

c) Sand Addition and Sampling: Dried, graded sand was first weighed, and then gradually added to the water in the reservoir while the pump was kept running to avoid precipitation and to encourage a homogeneous concentration in the system. It was noticed that when sand was added too quickly into the system, there was a high concentration buildup on the suction of the pump, resulting in unsteady flow characteristics. In order to measure the delivered concentration, the discharge was directed to a sampling bucket. Thus, by measuring the weight and volume of the delivered mixture, easy calculation of the flowing concentration was possible.

d) Miscellaneous: For steady flow, the pulsation dampener was utilized to reduce fluctuations in the pump output. Compressed air was supplied to the dampener and the water level was adjusted using the air regulator valve.

For unsteady or pulsating flow, the pulsation dampener was isolated from the flow circuit. The priming port was opened and the air was bled off from the collapsible tubing chamber of the pulser.

5.2 Testing Procedure

With the pump speed adjusted to give the desired flow rate, a weighed amount of sand was added to give a required concentration in the flow system. The flow was allowed to become stabilized at which time measurements were taken of reservoir temperature, flow rate and pressure drop across test section. A sample of delivered flow was taken for the steady flow at this point.

The sample was returned to the flow system and enough time was allowed for thorough mixing. Pulsed flow was initiated and the fluctuations of flow rate and pressure drop were recorded. Delivered concentration was again measured and the entire process was repeated for a higher sand concentration.

5.3 Test Conditions

There are two main objectives of the present research:

(1) To investigate the effect of velocity and concentration on the pressure drop along a vertical pipeline with solid-liquid flow.

(2) To study the effect of superposed pulsation frequency on the energy requirements of solid transport in a hydraulic lift line.

In order to achieve the first objective, steady flow experiments were conducted with slurries made of lime and three different sand compositions as given in Table (5-1). The flow velocity was varied between 0.76 to 3.35 m./sec. while the maximum volumetric

Sieve Designation	Sieve Opening (mm)	Percent Retained		
		Sand A	Sand B	Sand C
No. 4	4.76	0	0	0
No. 8	2.38	9.0	0	0
No. 10	2.00	23.0	0	0
No. 16	1.19	60.0	38.0	0
No. 20	0.841	-	52.0	2.3
No. 30	0.595	7.0	8.6	71.2
No. 40	0.420	-	-	22.4
No. 50	0.297	1.0	1.4	2.4
Weighted Average Diameter, d (mm)		1.84	1.20	0.66
Specific Gravity, S		2.62	2.65	2.58

Table (5-1) Physical Properties of Sand Used in the Experiments

concentration was 23.0 percent.

At high velocities and concentrations, however, the abrasive sand particles did considerable damage to the pump's rotor and stator. It was therefore decided that for pulsation experiments only low velocities and concentrations with Sand B should be used. Thus, the flow velocity was varied between 0.76 and 1.22 m./sec. while the maximum volumetric concentration was 10.0 percent. Pulsation frequencies used were 0.22 and 0.44 cycles per second.

CHAPTER 6

RESULTS AND DISCUSSION

6.1 Introduction

The experimental data and calculated results of steady and pulsating flows performed under the conditions described in Chapter 5 are presented in Appendix F, Tables (F-1) to (F-10).

The important parameters used in the graphical display of these results are the average mixture velocity $\overline{V}_m$, the pressure gradient $\frac{\Delta P}{\rho_w \Delta Z}$, and the delivered-volumetric concentration, C_s. The following evaluation is an attempt to define these parameters and to compare them with some of the other commonly used parameters.

6.1(a) Average Mixture Velocity $\overline{V}_m$

When refering to two phases flowing through conduits, the term velocity assumes various connotations. For dense solid particles being transported upwards by a liquid, it is usually considered that the tendency for these particles to settle results in the velocity of liquid being greater than that of the solids. The difference in these two velocities, normally referred to as the liquid-slip velocity, is a function of particle terminal settling velocity.

In other cases, velocities of solid and liquid phases are sometimes treated separately as though each phase is flowing

independently. In such a theoretical treatment of two phase flow, these velocities are referred to as the superficial velocities. Thus, the superficial velocity, V_{SL} of the liquid phase, in a sand-water mixture for example, is defined as

$$V_{SL} = \frac{4Q_L}{\pi D^2} \qquad (6.1)$$

Finally, if the two phases are considered to be flowing as one, the average mixture velocity $\bar{V}_m$ is simply derived as the average volume rate of mixture flow per unit cross-sectional area of pipe. Consequently, the average mixture velocity is relatively easy to determine and to visualize, therefore it is suitable for comparison of results.

6.1(b) Pressure Gradient $\frac{\Delta P}{\rho_w \Delta Z}$

The pressure drop encountered in vertical solid-liquid flow is mainly attributed to fluid-wall friction plus the potential energy required in lifting the mixture to some height above the datum. Since stability of flow was achieved prior to the recording of experimental data, kinetic energy effects due to acceleration of solids are considered negligible. Also, for convenience all pressure gradient data are expressed in units of metres of water per metre of test section height.

6.1(c) Delivered Volumetric Concentration C_s

Because of the disparity in solid and liquid velocities described in section 6.1(a), it is generally considered that the values of the delivered volumetric concentration C_s, and the transport volumetric concentration C_T are not the same. Actual measurements of transport concentration are scarce; and from limited experimental observations made by Cloete et al (1967) and Toda et al (1969), the difference between C_T and C_s appears to be minimal. The delivered concentration C_s can be measured directly by sampling the flow which emerges from the test section and may be expressed either as a percentage or a fraction of the total mixture volume.

6.2 Presentation of Results

(a) Steady Flow

Curves depicting the variation of pressure gradient with slurry mixture velocity at various flow concentrations are presented in Figures (6-1) to (6-7).

In general, all the steady flow curves for sand-water mixtures have a similar shape. At high velocities the curves tend to become parallel to one another and also the line for water while at low velocities they depart from the water line. And as expected, the higher the concentration of the solids in the mixture the higher the value of pressure gradient becomes at any given mixture velocity. This behaviour is typical for vertical slurry transport and the shape of the curves are similar to those obtained by Newitt et al (1961) with

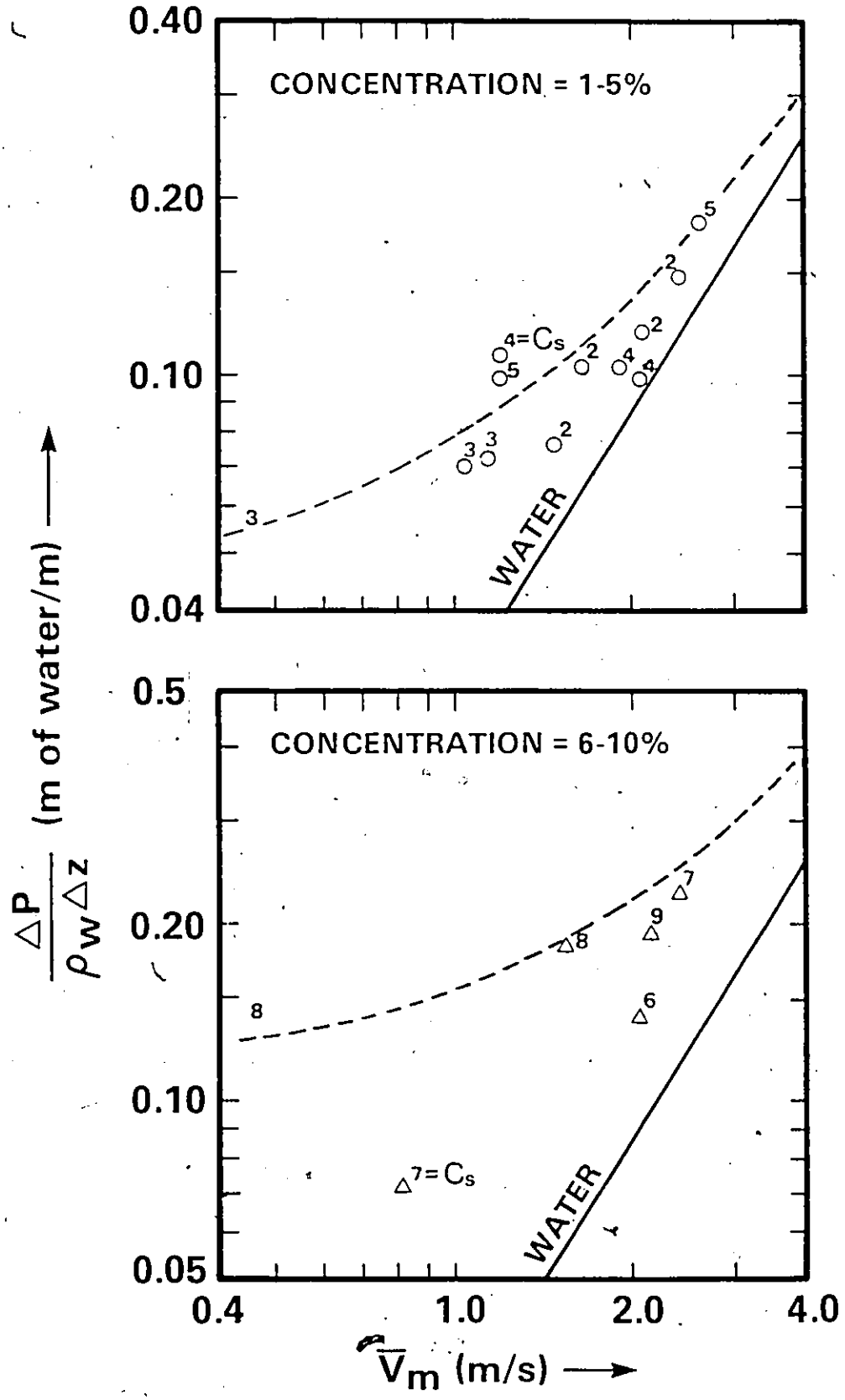

FIGURES (6.1) & (6.2) PRESSURE GRADIENT, SAND-A SLURRIES, IN TERMS OF C_s AND $\bar{V}_m$, d = 1.84 mm; S = 2.62 (- - - - Eq.2.3)

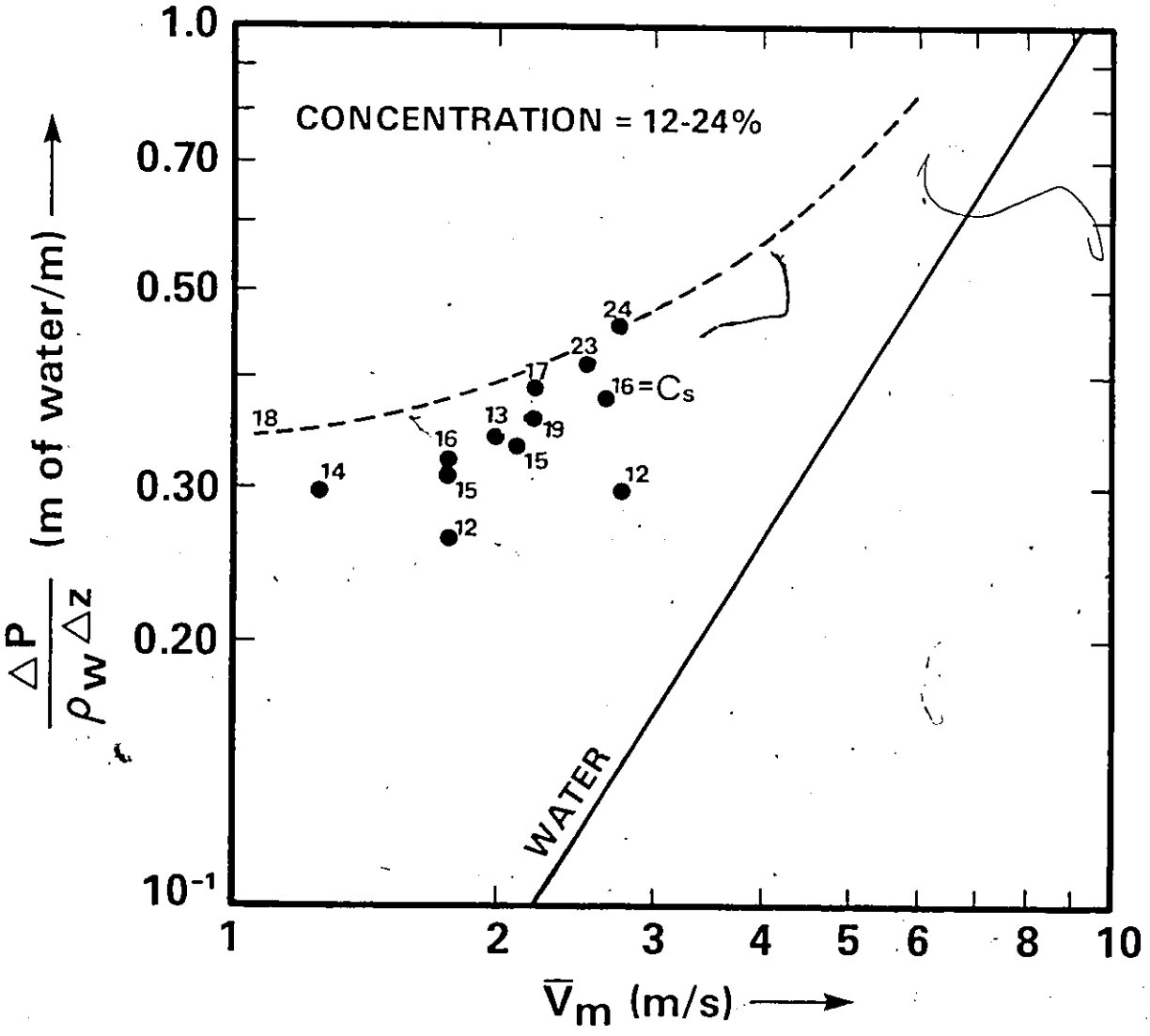

FIGURE (6.3) PRESSURE GRADIENT, SAND-A SLURRIES, IN TERMS OF C_s AND $\bar{V}_m$, d = 1.84 mm; S = 2.62 (---- Eq. 2·3)

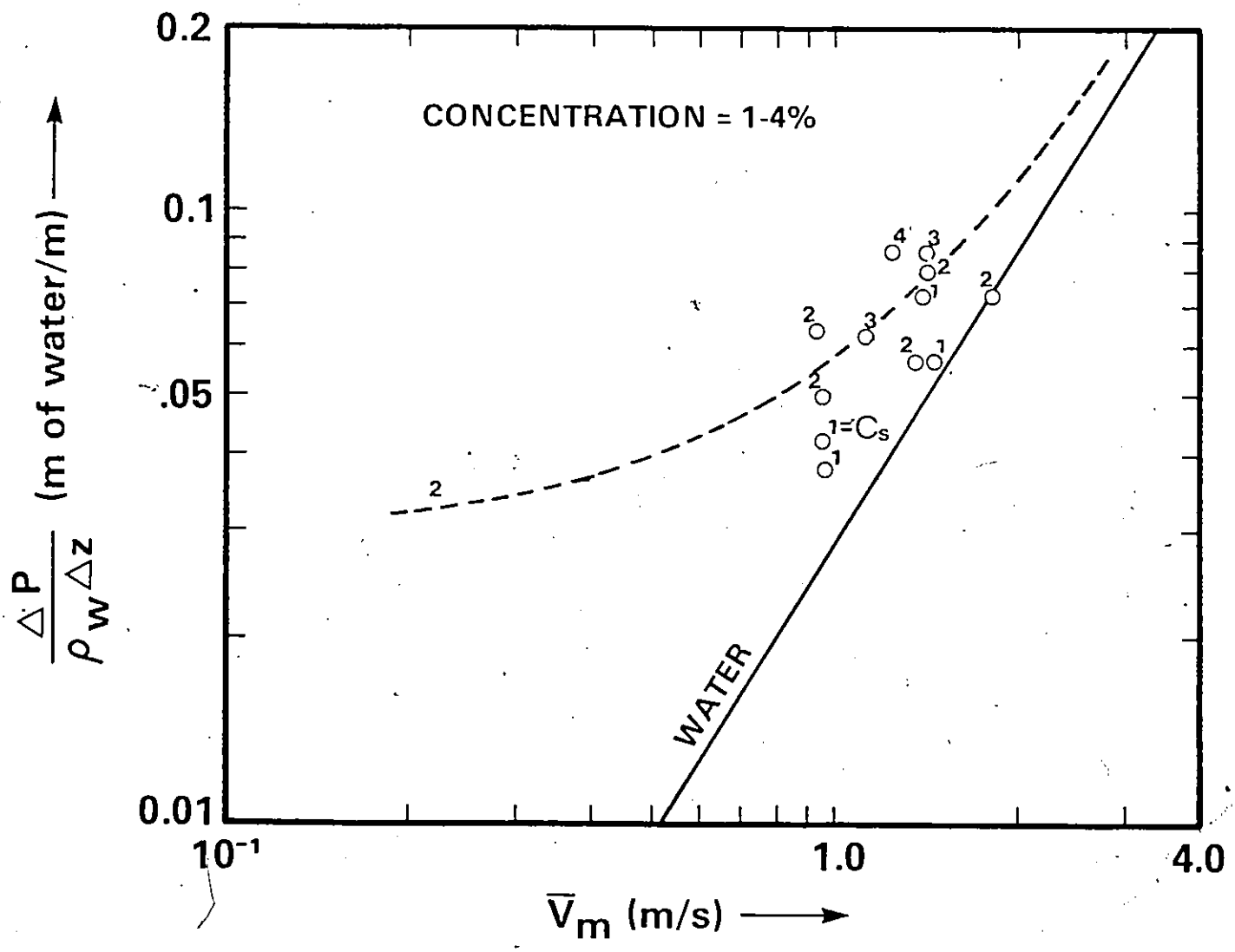

FIGURE (6.4) PRESSURE GRADIENT, SAND-B SLURRIES, IN TERMS OF C_s AND V_m, d = 1.20 mm; S = 2.65 (---- Eq.2·3)

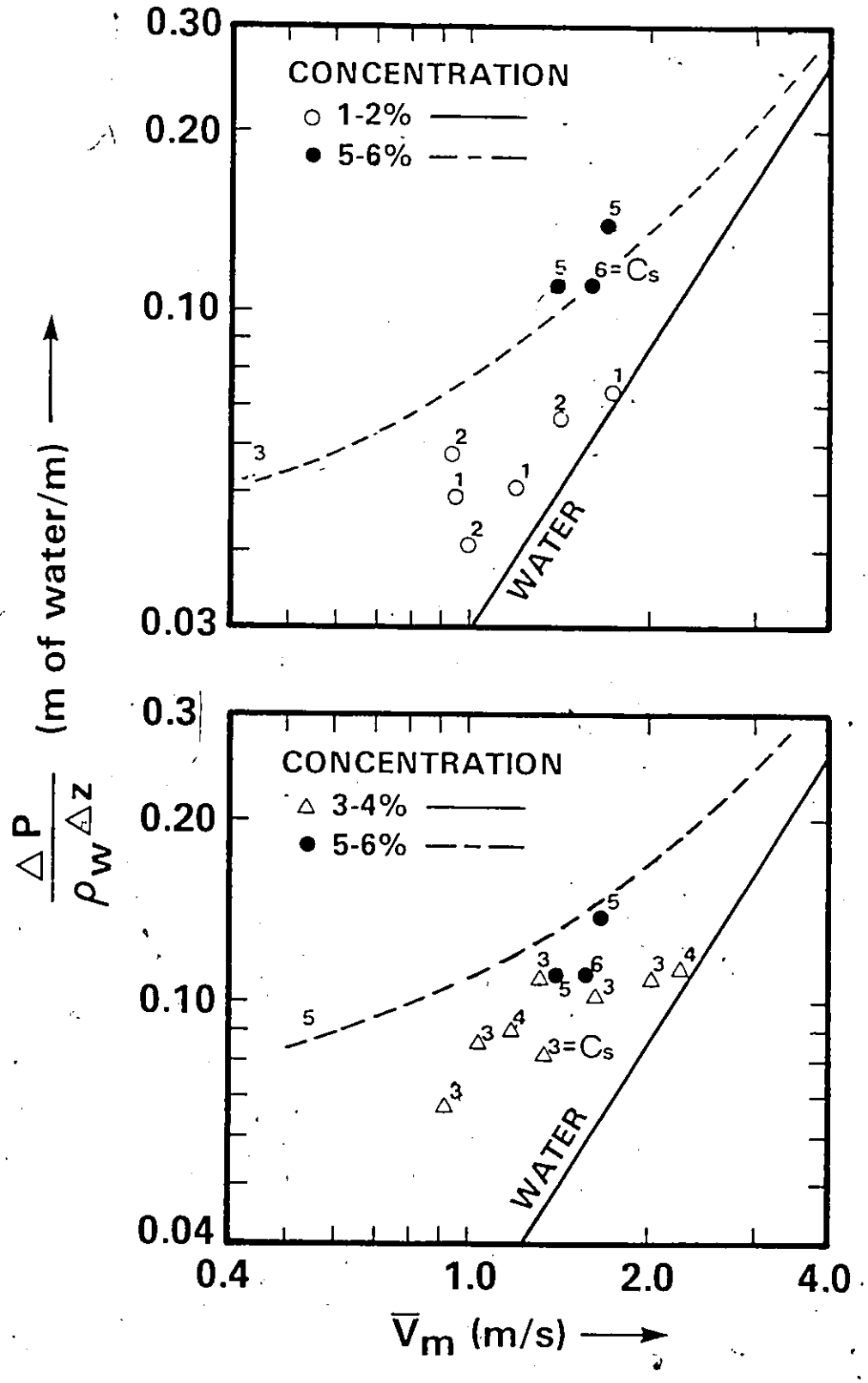

FIGURES (6.5) & (6.6) PRESSURE GRADIENT, SAND-C SLURRIES, IN TERMS OF C_s AND $\bar{V}_m$, d = 0.66 mm; S = 2.58 (- - - - Eq. 2·3)

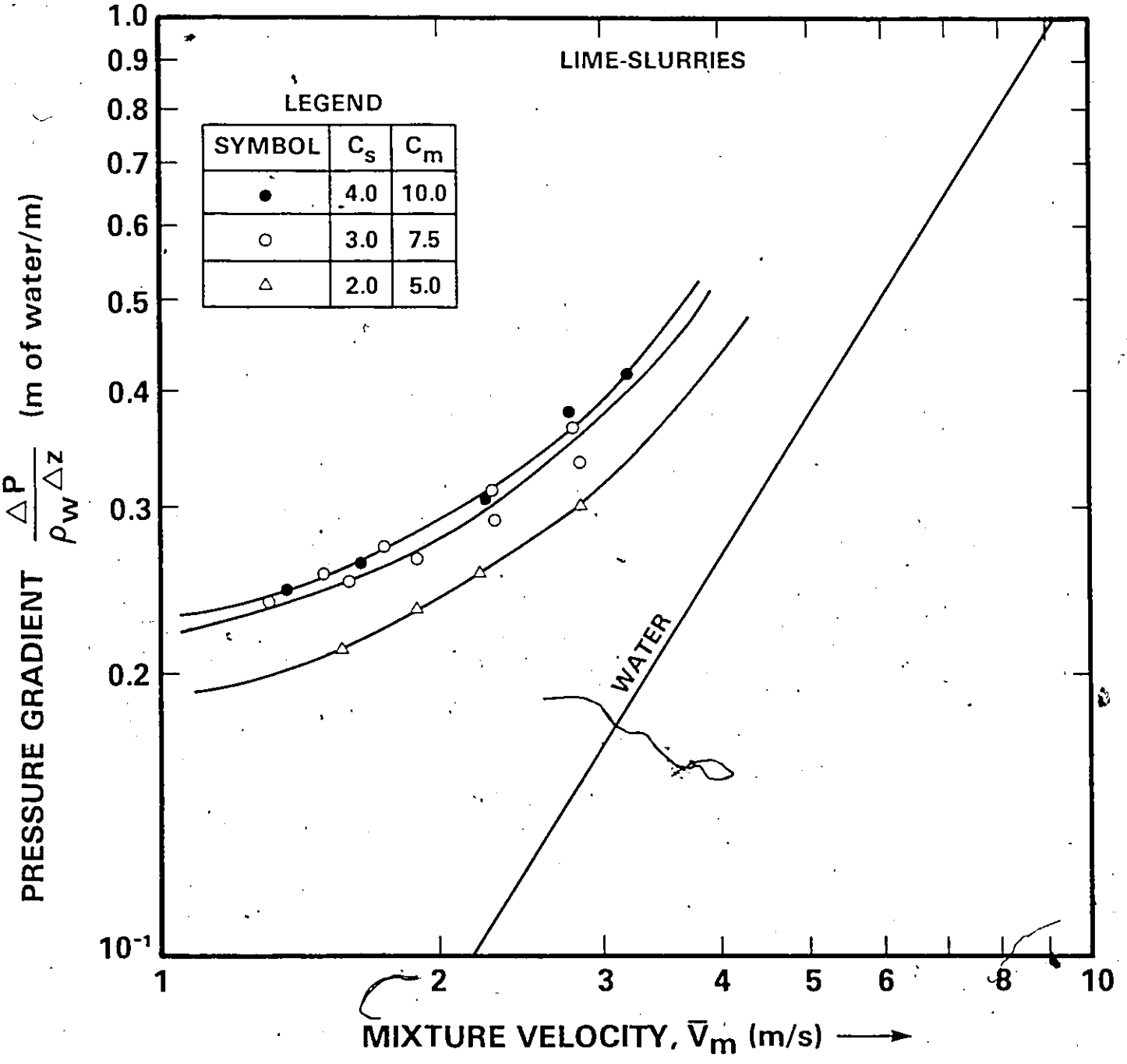

FIGURE (6.7) PRESSURE GRADIENTS, WATER-LIME SYSTEM, IN TERMS OF C_s AND $\bar{V}_m$.
d = 0.0018 mm; S = 2.35

sand-slurries in a 2.54 cm.-diameter pipe. More accurate results have been obtained by other researchers such as Toda et al (1969) with slurries of uniform diameter glass particles. In such experiments, it is apparent that particle collisions are fewer since all the particles tend to have the same slip velocity. In cases where the particles are spherical as well as uniform [Kopko et al (1975)], there is good agreement between experimental and theoretical results.

If we compare the curves for A, B and C sand-slurries at concentrations below 5.0%, it can be seen that the slurries consisting of smaller size particles yield slightly higher pressure drops at low mixture velocities. However, with lime slurries consisting of very fine particles, the pressure drop is considerably higher than for the sand slurries tested at the same concentration and velocity.

Since the specific gravity of lime (2.35) is less than that of sand (2.60), then an explanation of the increased pressure gradient must involve the effect which fine particles have on the pressure drop due to friction. On the other hand, very fine particles have been known to reduce the pressure gradient as will be discussed later on in this chapter. Newitt suggests that, since the diameter of fine particles are of the same order as the thickness of the laminar sub-layer at the pipe wall, they may influence the rate of shear; thus increasing the pressure drop.

Because of this solid-wall friction, higher pressure drops than expected may be obtained when pumping a sand-water mixture which consists basically of medium-sized sand but includes moderate amounts

of fine sand particles. A buildup of such particles in the re-circulating slurry may be the result of sand degradation caused by high pumping rates. This is exhibited in a deviation of data points along the best-fitted curves. Another reason for the deviation of data points is the difficulty involved in duplicating concentrations over a range of mixture velocities.

6.2(b) Pulsatile Flow

Results of the pulsatile flow experiments are given in Table (F-10) and Appendix A-2. They represent the flow conditions of superposed low frequency pulsation on the vertical transport of low concentration Sand-B suspensions in water.

As expected, the effect of pulsation on the overall pressure drop is insignificant when compared to the effect of the hydraulic head in upward vertical flow. This indicates that there is no advantage to be gained under these conditions. However, some benefit may be derived from the use of pulsatile flow in cases where the pressure drop due to friction and solid hold-up is substantial. According to Section 6.2(a) above, this would suggest that pulsatile flow may be advantageous with dense slurries of fine particles ($d < 0.25$ mm).

6.3 Data Correlation

The comparison of steady flow experimental data with the theoretical pressure gradient given by Equation (2-3) is shown in Figures (6-8) to (6-10). It can be seen from these graphs that the

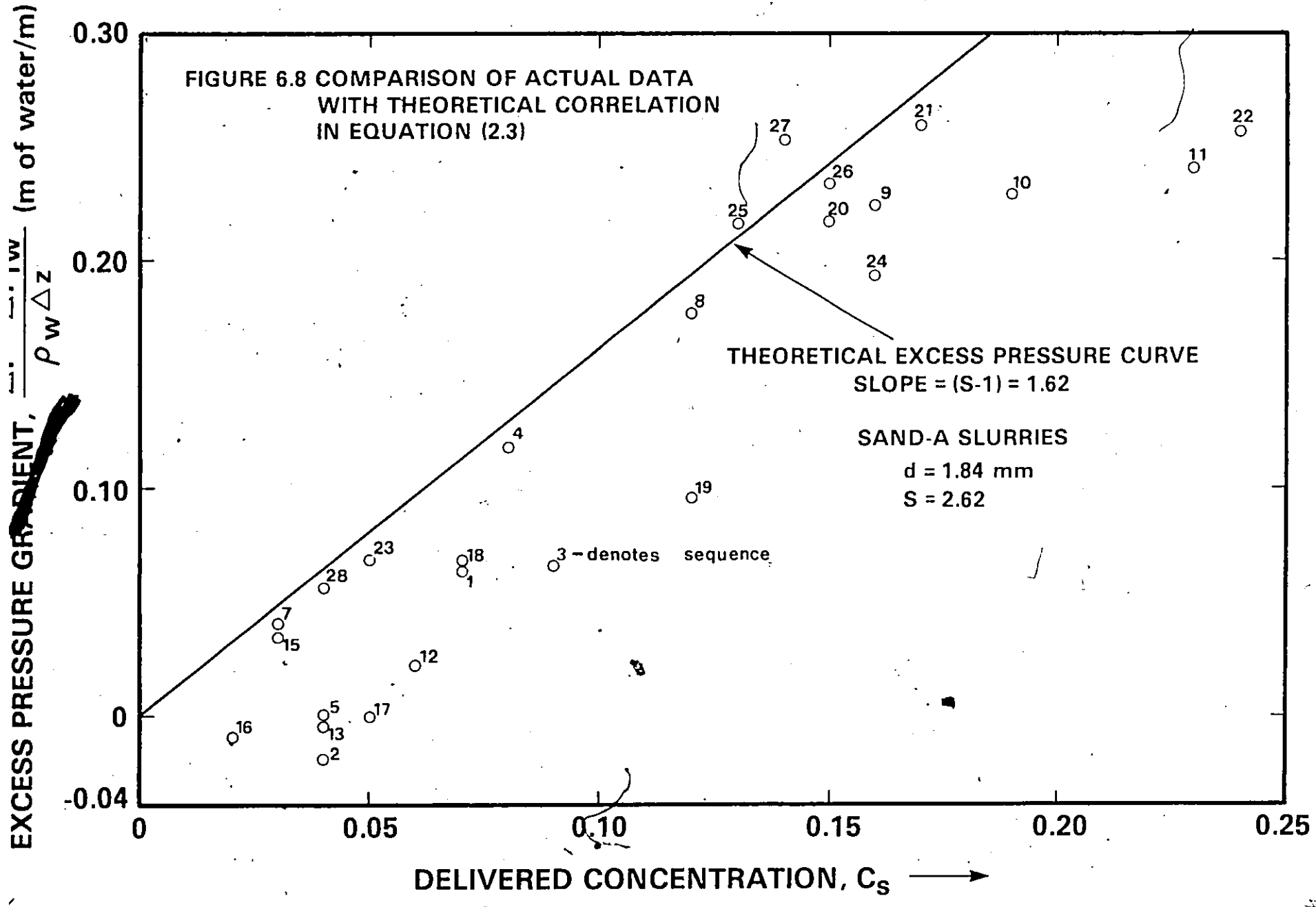
FIGURE 6.8 COMPARISON OF ACTUAL DATA WITH THEORETICAL CORRELATION IN EQUATION (2.3)
THEORETICAL EXCESS PRESSURE CURVE
SLOPE = (S-1) = 1.62
SAND-A SLURRIES
d = 1.84 mm
S = 2.62
3 – denotes sequence
EXCESS PRESSURE GRADIENT, $\frac{i - i_w}{\rho_w \Delta z}$ (m of water/m)
DELIVERED CONCENTRATION, C_s
0.30
0.20
0.10
0
-0.04
0
0.05
0.10
0.15
0.20
0.25

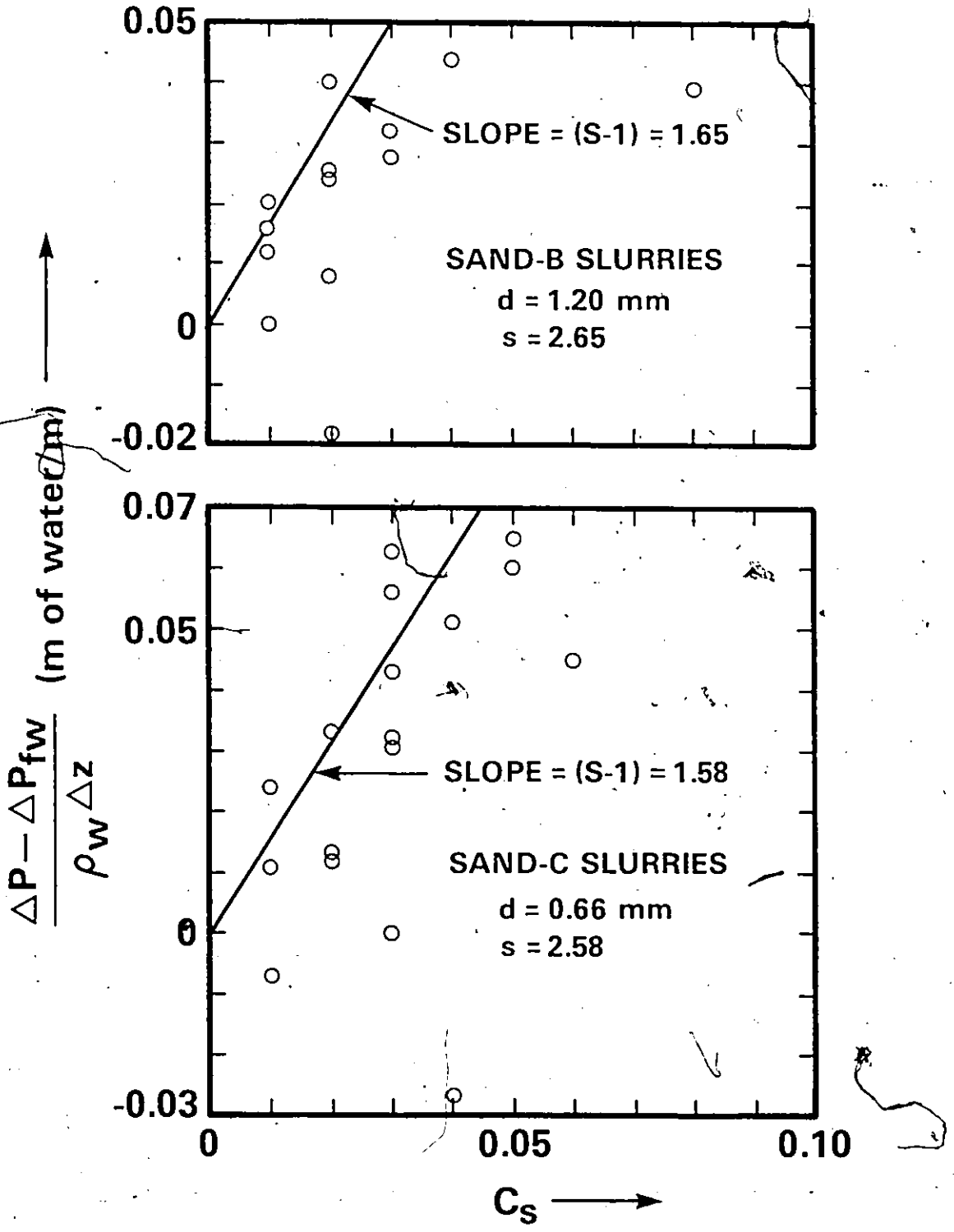

FIGURES (6.9) & (6.10). COMPARISON OF ACTUAL DATA WITH THEORETICAL CORRELATION IN EQUATION (2.3)

predicted excess pressure gradient gives an average error of +0.044, +0.020, and +0.017 for Sand-A, B and C respectively measured in metres of water per metre of test section height. These errors indicate the values by which the theoretical pressure gradient given by Equation (2-3) exceeds the experimental pressure gradient.

Similar results have been reported by Oedjoe et al (1966) with slurries of coarse gravel and coal particles in a 10.5 cm.-diameter vertical pipeline. Kopko et al (1975) also obtained average percentage errors of +6.3 and +1.5 for iron pellets of 1.86 and 3.33 mm.-diameter respectively. The iron pellets were hydraulically transported in a 6.1 cm.-diameter vertical pipeline.

If we consider that the total pressure drop consisting of the hydraulic head and frictional head loss is always greater than 1.0 metre of water per metre of test section height, then the average error is less than 4.0 percent for all the medium-sized sand suspensions in the present study. Therefore, this method of predicting pressure gradient using the theoretical excess pressure gradient presented by Equation (2.3) may be considered more suitable since it inherently provides a larger margin of safety.

For slurries of particles of diameter larger than 0.25 mm, Durand (1953) suggested that,

$$\Delta P_{fm} = \Delta P_{fw} \qquad (6.2)$$

The excess pressure gradient graphs indicate that, contrary to Equation (6-2), the frictional losses due to slurries are consistently slightly less than that of water flowing under the same conditions.

In the case of slurries consisting of fine particles, the lower frictional losses can be attributed to turbulence suppression [Brodkey (1967)]. However, there is no theoretical basis to account for this phenomenon in medium-sized sand suspensions apart from the size distribution in which the range extends to include fine particles.

Correlation curves which utilize the dimensionless parameters ϕ and ψ are shown in Figures (6-11) to (6-13). These parameters were used by Newitt et al (1961) to obtain the empirical equation (2-1) for fine particles ($d < 0.25$ mm). Although a more accurate empirical relationship was obtained using this method, slurries with Sand A, B and C yielded unique solutions with slopes of 2.79, 6.59 and 4.32 respectively.

Figures (6-11), (6-12) and (6-13) show that a universal correlation between ϕ and ψ is not feasible for medium-sized sand slurries since they cannot be applied for slurries other than those from which they were obtained.

Experiments were carried out using lime slurries in order to verify Equation (2-1) for slurries of particles of diameter less than 0.25 mm. The data presented in Figure (6-14) indicate that the empirical equation obtained by Newitt et al (1961) is apparently not valid for lime slurries ($d = 0.0018$ mm.). Whereas the slope obtained by Newitt was approximately 1.00, the line which best fitted the data for lime slurries gave a slope of approximately 2.59.

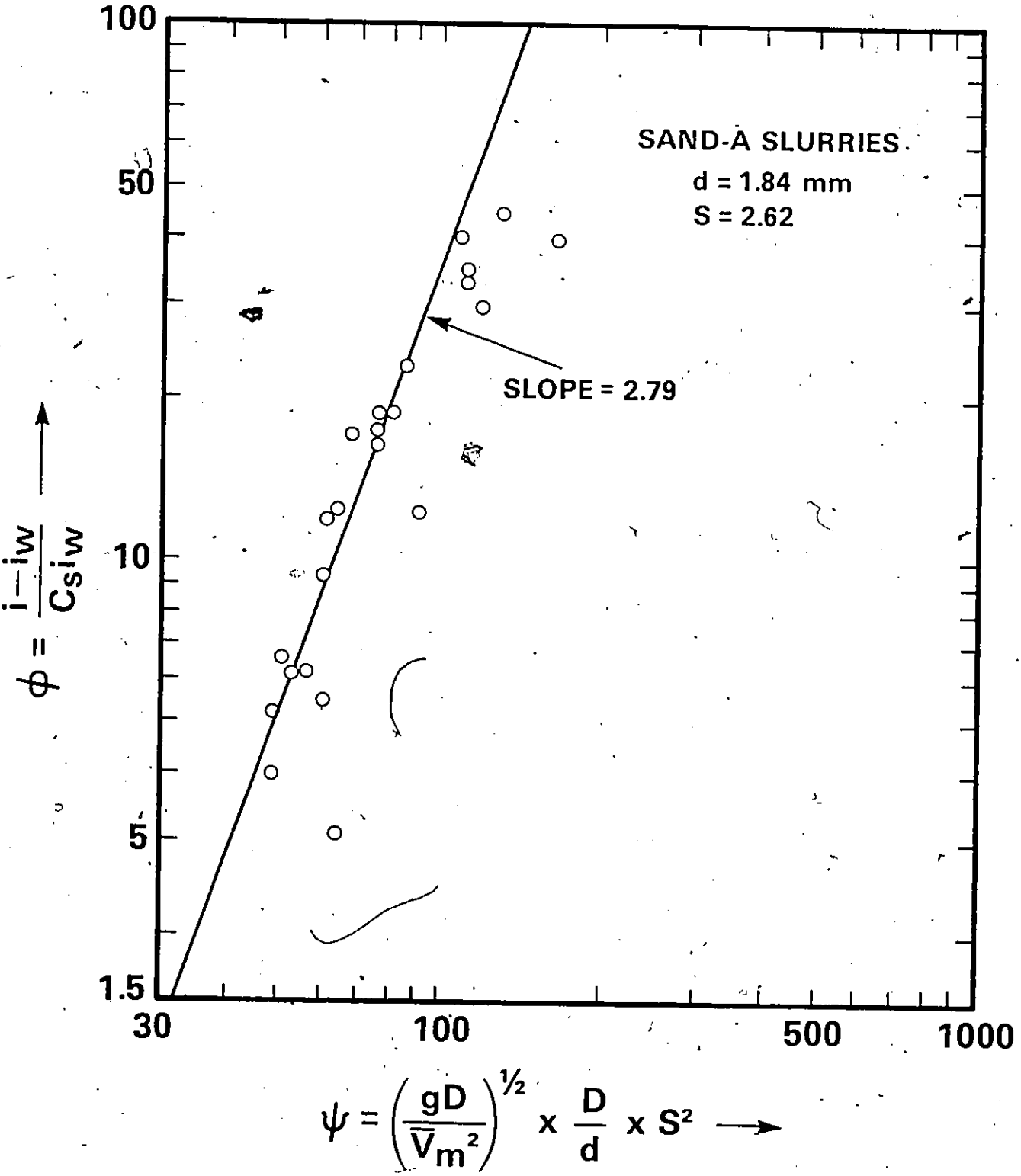

FIG. (6.1.1) CORRELATION CURVE FOR SAND-A SLURRIES USING PARAMETERS ϕ AND ψ

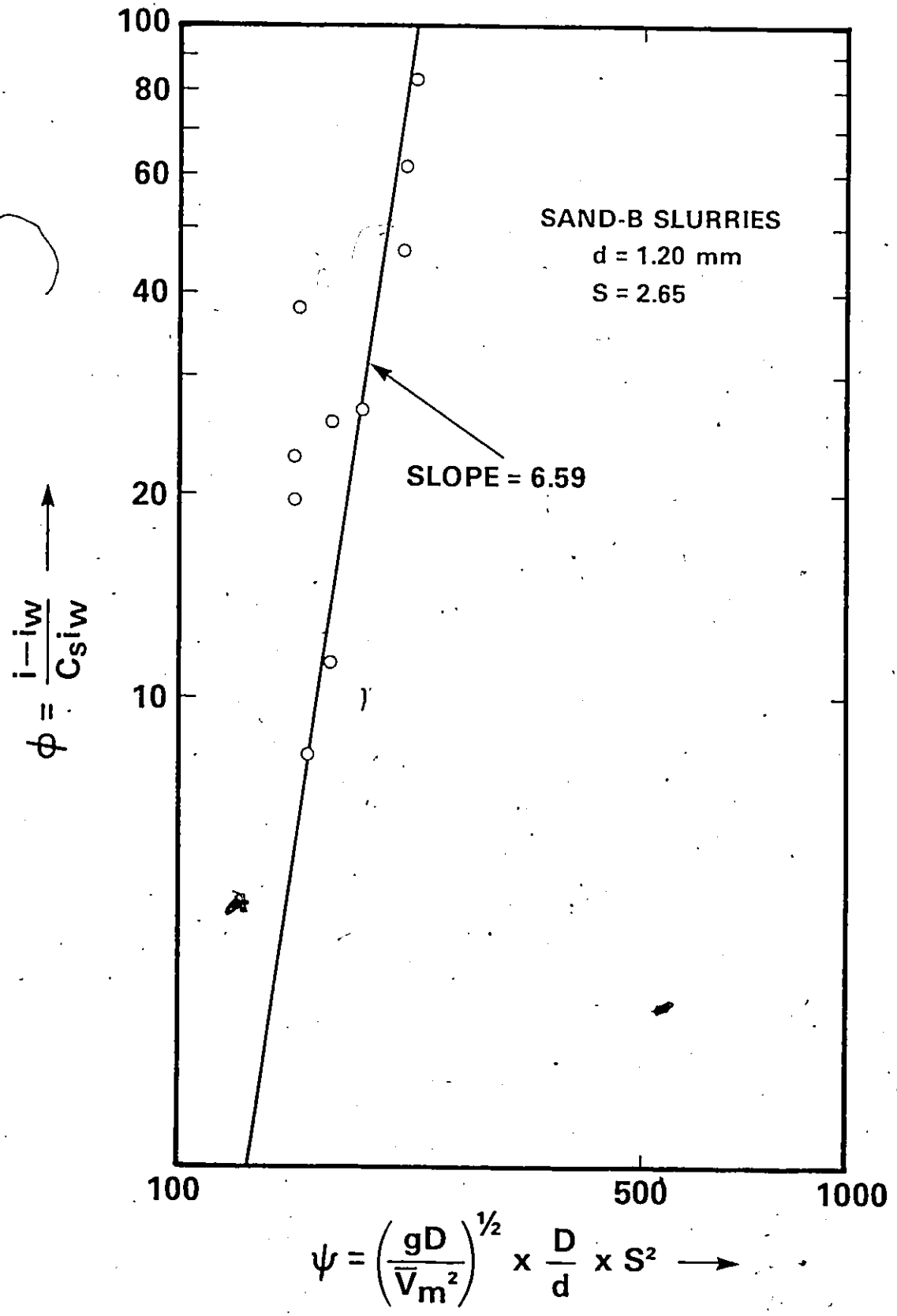

FIG. (6.12) CORRELATION CURVE FOR SAND-B SLURRIES USING PARAMETERS ϕ AND ψ

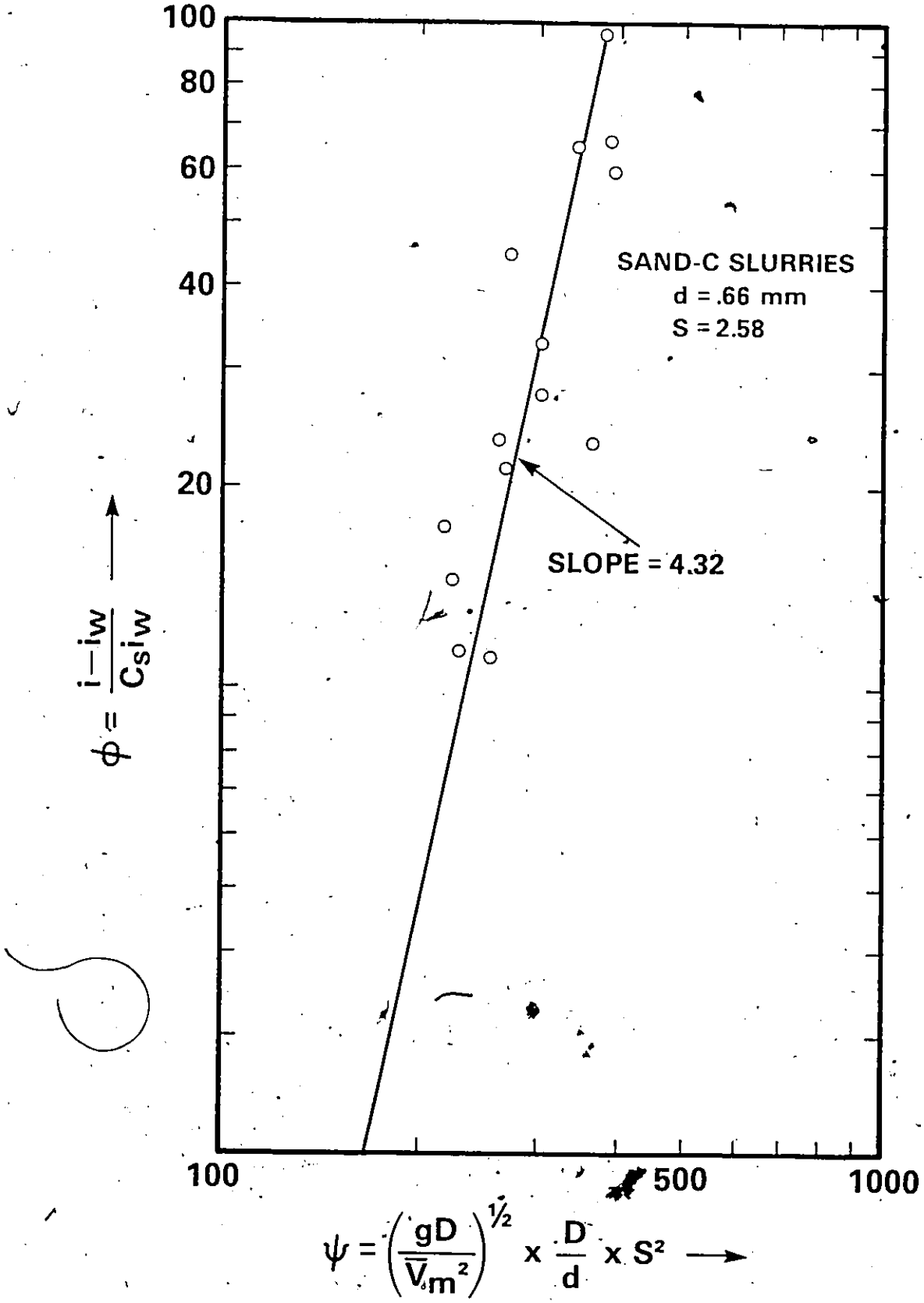

FIG. (6.13) CORRELATION CURVE FOR SAND-C SLURRIES USING PARAMETERS ϕ AND ψ

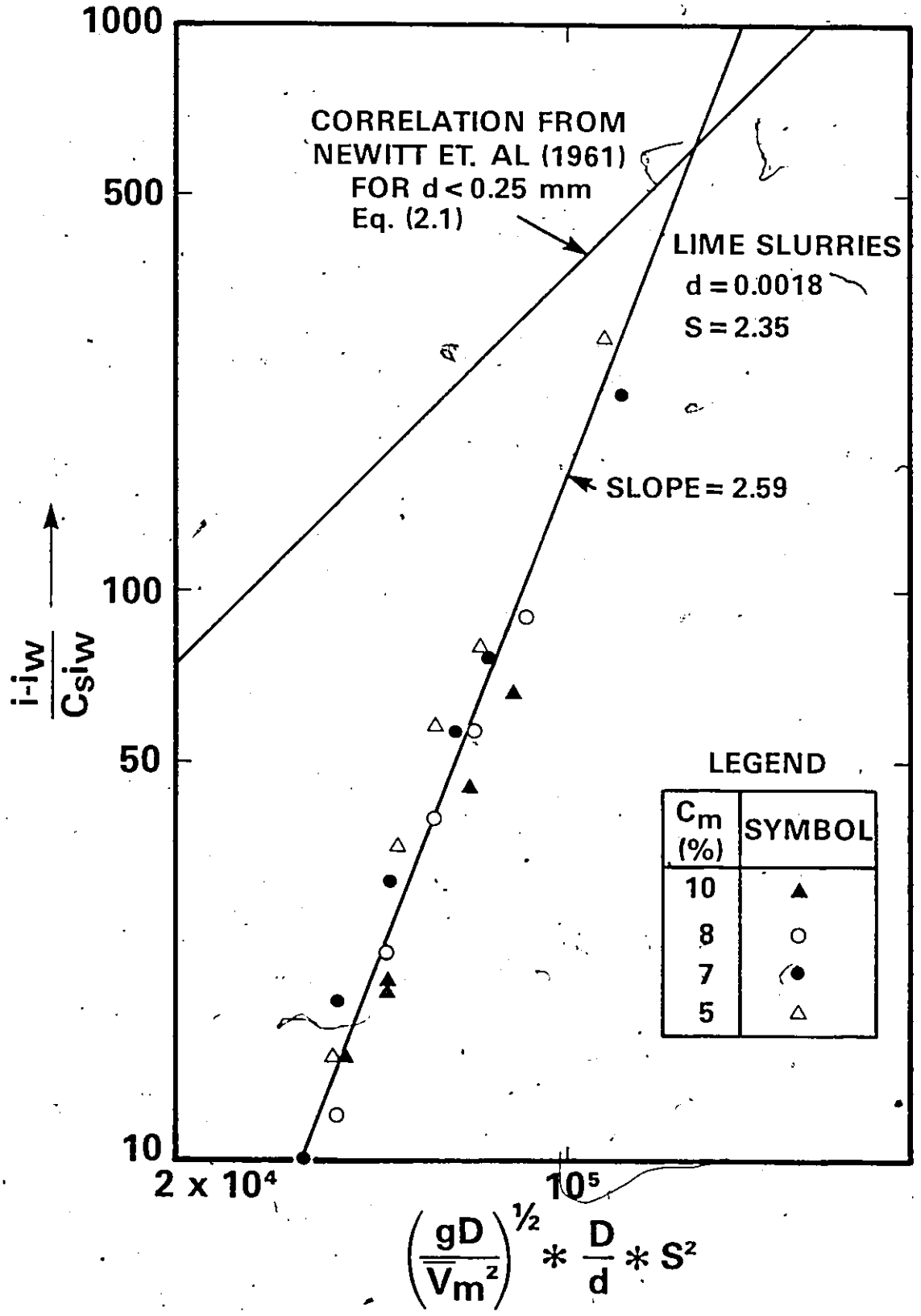

FIG. (6.14) CORRELATION CURVE FOR LIME SLURRIES

Figure (6-14) shows that for the same mixture velocity, the pressure gradient predicted by Newitt's correlation in Equation (2-1) will be greater than the present data for lime slurries. This indicates that the size of the lime slurry particles appears to be outside the range of particle sizes for which Equation (2-1) is valid. The lower pressure gradient may be the result of a drag reduction phenomenon more commonly associated with the viscoelastic effects exhibited by water solutions of long-chain polymers.

CHAPTER 7

CONCLUSIONS AND RECOMMENDATIONS

7.1 Conclusions

Based on the available experimental collected data and the analysis of these results presented in this thesis, the following conclusions can be made.

(a) The pressure gradient 'i' of a slurry being transported vertically upwards in a pipeline is dependent upon the particle average weighted diameter 'd' as well as the distribution range of the solids. That is, for similar flow conditions, the pressure gradient decreases as d increases.

(b) The pressure gradient of medium-sized sand slurries can be relatively accurately predicted by determining the frictional pressure drop due to water flowing under similar conditions and adding the excess hydrostatic pressure drop due to the presence of solids.

(c) The empirical equation obtained by Newitt et al (1961) given by Equation (2-1) for slurries of particles of diameter less than 0.25 mm. does not appear to be valid when the particle diameter of the slurry is of the order of or less than 2.0 microns.

(d) There appears to be no benefit to be derived by superposing pulsations on the steady flow of low concentration slurries of medium-sized particles in a vertical pipeline since the frictional

pressure drop is small when compared to the overall pressure drop.

7.2 Recommendations

Recommendations for further studies are listed as follows.

(a) Experiments should be conducted to obtain the limit of applicability of Newitt's equation for slurries of particles of various sizes and shapes.

(b) Pulsatile flow experiments should be carried out with dense slurries of fine particles so as to determine whether energy savings are possible at low frequencies (0 ~ 0.25 cycles per second) and high concentrations in vertical pipelines.

(c) It is important that studies be carried out concerning the role of particle size distribution and particle shape in the turbulent flow regime for steady and unsteady vertical flow of slurries. It is hoped that such studies would reveal the effect that particles of various sizes exert on the overall flow turbulence and to the flow region adjacent to the walls of the pipeline.

APPENDIX A

SAMPLE CALCULATION

A-1 Steady Flow Measurements

The readings for steady flow taken on June 16, 1980, with the Sand-B slurry were chosen arbitrarily to illustrate a typical calculation (Table A-1). The calculated results which are presented in tabular form along with the experimental data in Appendix F were determined in a similar manner to the following sample calculation.

The Average Mixture Velocity, $\overline{V}_m$

$\overline{V}_m$ was calculated according to the following equation:

$$\overline{V}_m = \frac{\text{flow rate}}{\text{pipe cross-sectional area}}$$

$$\text{Flow rate (m/s)} = Q\,(\%) \times \frac{178}{100}\,(\text{US GPM}) \times \frac{1}{60}\left(\frac{\text{min}}{\text{sec}}\right) \times 0.00378\left(\frac{\text{m}^3}{\text{US Gal.}}\right)$$

where 178 US GPM = 100% Max$^{\text{m}}$ Flow Rate (see Appendix B for Calibration Curves)

$$\text{Thus, } \overline{V}_m = Q\,(\%)\ \frac{\left[\frac{178}{100} \times \frac{1}{60} \times 0.00378\right]}{\pi/4\ (0.051)^2}$$

$$= Q\,(\%) \times 0.055 \qquad \text{(A-1)}$$

Since the percentage flow rate as indicated by the flowmeter was 17.5%, from equation (A-1)

Then $\overline{V}_m = 17.5 \times 0.055 = 0.96$ (m/s)

The Pressure Gradient, i:

In order to analyse the accuracy of the pressure difference measurements across the test section as determined using the mercury manometer, we refer to the system as shown in Figure (A-1).

Equating the pressure at points (1) and (2) in the mercury columns, the following general equation is obtained:

$$P_{(A)} - P_{(B)} = \Delta H_m (\rho_{Hg} - \rho_{wa}) g + \Delta Z \rho_{wa} g \qquad (A-2)$$

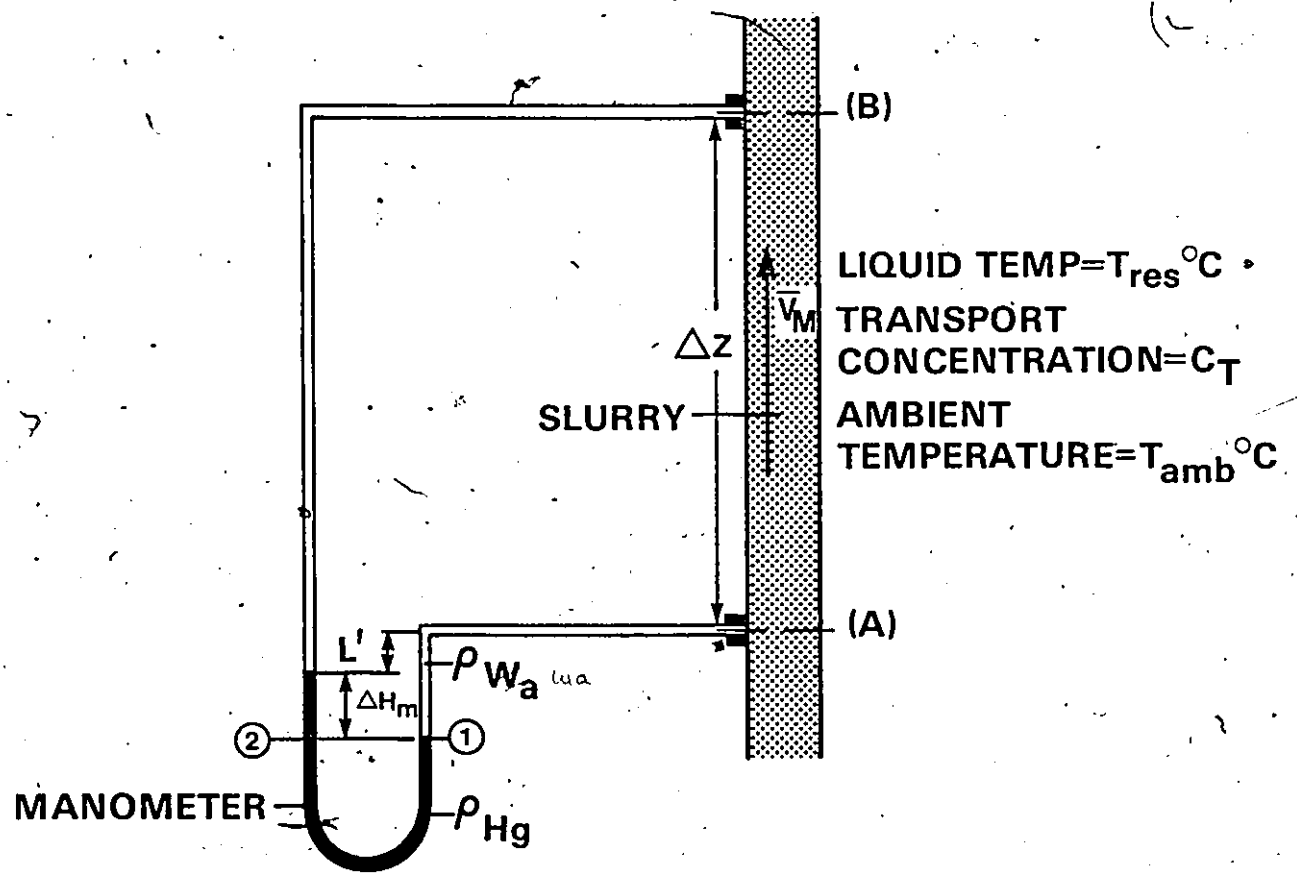

FIG. (A-1) PRESSURE DIFFERENCE MEASUREMENT

TABLE A-1: Sample Work Sheet

Data Point	Sand Used	Avg. Diam.	Performed By	Date
40	Sand-B	1.20 mm	B. Joel	16/6/80

Indicated Flowrate, Q	=	17.5	(%)
Manometer Reading, ΔH_m	=	0.341	(in Hg)
Ambient Temperature, $T_{amb.}$	=	20.0	(^oC)
Reservoir Temperature, $T_{res.}$	=	23.2	(^oC)
Weight of Sample, W	=	26 (lbs)	14 (oz)
Volume of Sample, v	=	11.90	(litres)

For a slurry of transport volumetric concentration, C_T, flowing with some finite velocity, $\overline{V}_m$, the L.H.S. of equation (A-2) can be approximated as follows:

$$P_{(A)} - P_{(B)} \simeq \Delta P_{fm} + \Delta Z\, \rho_{mr}\, g \qquad (A-3)$$

which can be rearranged to give

$$\frac{\Delta H_m}{\Delta Z}\left(\rho_{Hg}/\rho_{wr} - \left(\frac{\rho_{wa}}{\rho_{wr}}\right)\right) = \frac{\Delta P_{fm}}{\Delta Z\, \rho_{wr}\, g} + \left(\frac{\rho_{mr}}{\rho_{wr}} - 1\right) - \left(\frac{\rho_{wa}}{\rho_{wr}} - 1\right)$$

If $i \equiv \dfrac{\Delta P_{fm}}{\Delta Z \rho_{wr} g} + \left(\dfrac{\rho_{mr}}{\rho_{wr}} - 1\right)$

then $i = \dfrac{\Delta H_m}{\Delta Z}\left(\rho_{Hg}/\rho_{wr} - 1\right) + \left(\rho_{wa}/\rho_{wr} - 1\right)$

$$= \Delta H_m \text{ (in Hg)} \times \frac{0.0254}{2.227}\,(13.6-1) + \left(\rho_{wa}/\rho_{wr} - 1\right)$$

$$= \Delta H_m \text{ (in Hg)} \times 0.1437 + \left(\rho_{wa}/\rho_{wr} - 1\right) \qquad (A-4)$$

Since the manometer reading was 0.341 in Hg, at $T_{amb} = 20.0^{\circ}C$

and $T_{res} = 23.2\ ^{\circ}C$ and,

Density* of water at 23.2°C $= \rho_{wr} = 0.99752 \times 10^3$ (kg/m^3)

Density of water at 20.0°C $= \rho_{wa} = 0.99823 \times 10^3$ (kg/m^3)

From equation (A-4),

$$i = 0.341 \times (0.1437) + \left(\frac{0.99823}{0.99752} - 1\right)$$

$$= 0.049 + 0.0007$$

$$= 0.050 \text{ (m of water /m)}$$

The Delivered Concentration, C_s:

The delivered volumetric concentration, C_s, was calculated according to the following equation:

$$C_s = \left(\frac{\rho_{mr}}{\rho_{wr}} - 1\right) / \left(\frac{\rho_s}{\rho_{wr}} - 1\right) \qquad \text{(A-5)}$$

where $\rho_{mr} = \dfrac{\text{Weight of delivered sample}}{\text{Volume of delivered sample}}$

such that $\rho_{mr} = \dfrac{W \text{ (lbs)} \times 0.4539}{v \text{ (litres)} \times 10^{-3}}$ (A-6)

---

* Taken from "Chemical Engineers' Handbook" 4th Edition by John H. Perry. Table 3-46.

Since the weight and the volume of the delivered sample were 26.875 pounds and 11.90 litres respectively, equation (A-6) gives

$$\rho_{mr} = \frac{26.875 \times 0.4539}{11.90 \times 10^{-3}}$$

$$= 1.0251 \times 10^{3} \ (kg/m^{3})$$

Then, $C_s = \left(\frac{1.0251}{0.99752} - 1\right) / (2.65 - 1) = 0.017$

The Reynolds Number, Re:

Re was calculated according to the following equation:

$$Re = \frac{\rho_{wr} \overline{V}_m D}{\mu_{wr}} \qquad (A-7)$$

$$= \frac{\rho_{wr} \ (kg/m^3) \times \overline{V}_m \ (m/s) \times 0.051 \ (m)}{\mu_{wr} \ (centipoise) \times 10^{-3}}$$

Since the viscosity of water μ_{wr} at 23.2°C was 0.9315 centipoise and $\overline{V}_m$ was 0.96 m/s, equation (A-7) gives

$$Re = \frac{(0.99752 \times 10^{3}) \times 0.96 \times 0.051}{0.9315 \times 10^{-3}} = 52\,430$$

The Water Pressure Gradient, i_w:

i_w represents the pressure gradient of water flowing through the test section under similar conditions of average velocity and temperature as that for the slurry and was calculated from the following equation:

$$i_w = \frac{\Delta P_{fw}}{\Delta Z \rho_{wr} g} = f \times \frac{1}{D} \times \frac{\overline{V}_m^2}{2g} \qquad \text{(A-8)}$$

where f is the friction factor determined from Figure D-1, Appendix D.

Equation (A-8) gives,

$$i_w = f \times \frac{1}{0.051} \times \frac{\overline{V}_m^2}{2 \times 9.81}$$

$$= \frac{f \times \overline{V}_m^2}{1.00062}$$

Since at Re = 52,430, f = 0.028 and $\overline{V}_m$ = 0.96 m/s.

$$i_w = \frac{0.028 \times (0.96)^2}{1.00062}$$

$$= 0.026 \text{ (m of water/m)}$$

A-2 Calculation of J_p'/J_s

For steady flow, the dissipation energy per mass flow rate per unit length of pipe, J_s is calculated from the following equation:

$$J_s = \left[\frac{\frac{\pi}{4} D^2 \Delta P_T \overline{V}_m}{\Delta Z} \right] \Big/ \frac{\pi}{4} D^2 \overline{V}_m \rho_{mr} g$$

$$= \frac{\Delta P_T}{\Delta Z \rho_{mr} g} \qquad \text{(A-9)}$$

such that, $$\frac{\Delta P_T}{\Delta Z \rho_{mr} g} = \frac{\Delta P}{\Delta Z \rho_{mr} g} + \frac{\rho_{wa}}{\rho_{mr}}$$

$$= i \times \left(\frac{\rho_{wr}}{\rho_{mr}} \right) + \left(\frac{\rho_{wa}}{\rho_{mr}} \right) \qquad \text{(A-10)}$$

For pulsed flow, the dissipation energy over a cycle per unit length of pipe, J_p', can be expressed as follows:

$$J_p' = \frac{\omega}{2\pi} \cdot \frac{1}{\Delta Z} \int_0^{2\pi/\omega} \frac{\pi}{4} D^2 \Delta P_T(t) \overline{V}_m \, dt \qquad \text{(A-11)}$$

such that, $$J_p = J_p'/\dot{m} = \frac{\omega}{2\pi} \cdot \frac{1}{\Delta Z} \int_0^{2\pi/\omega} \frac{\pi D^2}{4} \Delta P_T(t) \overline{V}_m \, dt \Big/ \frac{\pi}{4} D^2 \overline{V}_m \rho_{mr} g$$

$$= \frac{\omega}{2\pi} \cdot \frac{1}{\Delta Z \rho_{mr} g} \int_0^{2\pi/\omega} \Delta P_T(t) \, dt \qquad \text{(A-12)}$$

If n is the number of time intervals in one cycle and summing the P_T's over that cycle, equation (A-11) can be computed as follows:

$$J_p' = \frac{1}{n\Delta T} \cdot \frac{1}{\Delta Z} \sum_{j=1}^{j=n} \overline{\Delta P}_{Tj} \frac{\pi}{4} D^2 \overline{V}_m \Delta t$$

where $$\overline{\Delta P}_{Tj} = \frac{1}{2}\left[\Delta P_{Tj} - \Delta P_{Tj-1}\right]$$

and $$\frac{\Delta P_{Tj}}{\Delta Z \rho_{mr} g} = \left[i \times \left(\frac{\rho_{wr}}{\rho_{mr}}\right) + \left(\frac{\rho_{wa}}{\rho_{mr}}\right)\right]$$

Thus equation (A-12) yields:

$$J_p = J_p'/\rho_m = \frac{1}{n\Delta t} \times \frac{1}{\Delta Z \rho_{mr} g} \sum_{j=1}^{j=n} \overline{\Delta P}_{Tj} \Delta t$$

since $$n\Delta t = \frac{1}{\omega}$$

then $$J_p = \frac{\omega \Delta t}{\rho_{mr}} \sum_{j=1}^{j=n} (\overline{i}_T \times \rho_{wr} + \rho_{wa})_j \qquad \text{(A-13)}$$

ω = 0.44 cycles per second.

The pulsed flow readings (Figure A-2) taken on May 29, 1980, with Sand-B slurry were obtained to demonstrate the operation of the pulser mechanism. The following is a typical caloulation.

MAY 29, 1980

PULSED FREQUENCY ω = 0·44 CYCLES/SEC.

T_{amb} = 21·0 °C

T_{res} = 17·0 °C

W = 31 lbs 6½ oz

v = 13·25 litres

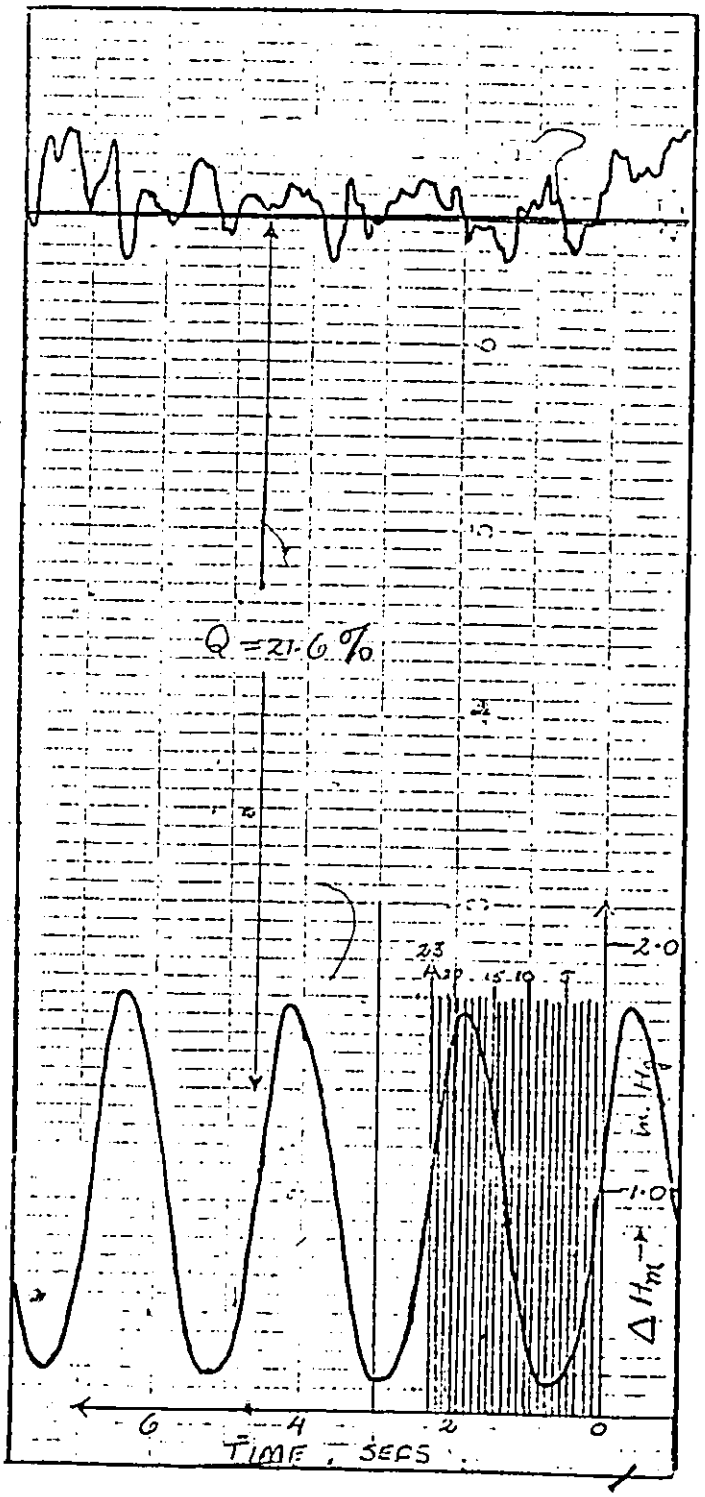

FIGURE (A-2). Sample Work Sheet and Pulsed-Flow Trace

J_p was calculated according to equation (A-13). Since $\Sigma\Delta\bar{H}_{mj} = 18.65$, $\bar{i}_T$ was obtained from equation (A-4) as follows:

$$\bar{i}_T = \Sigma\Delta H_{mj} \times 0.1437 + nx\left(\frac{\rho_{wa}}{\rho_{wr}} - 1\right)$$

$$= (18.65 \times 0.1437) + 23 \times \left(\frac{0.99802}{0.99880} - 1\right)$$

$$= 2.662 \text{ (m of water/m)}$$

$$\rho_{mr} = \frac{W \times 0.4539}{v \times 10^{-3}} = \frac{31.40625 \times 0.4539}{13.25 \times 10^{-3}} = 1.0759 \times 10^3 \text{ (kg/m}^3\text{)}$$

$$C_s = \left(\rho_{mr}/\rho_{wr} - 1\right) \Big/ (S - 1) = \left(\frac{1.0759}{0.9988} - 1\right) / 1.65$$

$$= 0.047$$

Thus $J_p = \frac{1}{23 \times 1.0759 \times 10^3} \times [2.662 \times 0.9988 \times 10^3 + 0.99802 \times 10^3 \times 23]$

$$= 1.035 \text{ (m of water/m)}$$

Now J_s was calculated using equation (A-10) in the following manner.

Since Q was 21.6%

then $\bar{V}_m = Q \times 0.055 = 1.188$ (m/s)

giving $\psi = (211.1) / \overline{V}_m = 178$

and $Re = \dfrac{1.188 \times (0.9988 \times 10^3) \times 0.051}{1.0828 \times 10^{-3}} = 55,888$

from Figure D-1, $f = 0.0279$

$$i_w = f \times \frac{1}{D} \times \frac{V_m^2}{2g}$$

$$= 0.0279 \times \frac{1}{0.051} \times \frac{(1.188)^2}{2 \times 9.81} = 0.039 \text{ (m of water/m)}$$

from Figure 6.12, at $\psi = 178.0$, $\phi = 18.5$

Hence, $i = C_s i_w \times \phi + i_w$

$$= 0.047 \times 0.039 \times 18.5 + 0.035$$

$$= 0.073 \text{ (m of water/m)}$$

$$J_s = 0.073\left(\frac{0.9988}{1.0759}\right) + \left(\frac{0.99802}{1.0759}\right)$$

$$= 0.995$$

$$J_p/J_s = \frac{1.035}{0.995} = 1.04$$

at $\omega = \dfrac{1}{n\Delta t} = \dfrac{1}{23 \times 0.0987} = 0.44$ (cycles per second)

ω = 0.22 cycles per second.

The pulsed flow readings taken on May 28, 1980 with Sand-B slurry were chosen arbitrarily to illustrate a typical calculation for the data presented in Figure (A-3).

J_p was calculated according to equation (A-13). Since $\Sigma\overline{\Delta H}_{mj}$ = 8.451, $\overline{i}_T$ was obtained from equation (A-4) as follows:

$$\overline{i}_T = \Sigma\overline{\Delta H}_{mj} \times 0.1437 + n \times \left(\frac{\rho_{wa}}{\rho_{wr}} - 1\right)$$

$$= (8.451 \times 0.1437) + 15 \times \left(\frac{0.99802}{0.99843} - 1\right)$$

$$= 1.208 \text{ (m of water/m)}$$

and $\rho_{mr} = \dfrac{W \times 0.4539}{v \times 10^{-3}} = \dfrac{16.8125 \times 0.4539}{7.5 \times 10^{-3}} = 1.0175 \times 10^3 \text{ kg/m}^3$

$$\therefore \quad C_s = \left(\rho_{mr}/\rho_{wr} - 1\right) \Big/ (s - 1) = \left(\frac{1.0175}{0.99843} - 1\right) \Big/ 1.65$$

$$= 0.011$$

Thus, $J_p = \dfrac{1}{15 \times 1.0175 \times 10^3} [1.208 \times 0.99843 \times 10^3 + 0.99802 \times 10^3 \times 15]$

$$= 1.060 \text{ (m of water/m)}$$

J_s was calculated using equation (A-10) in the following manner.

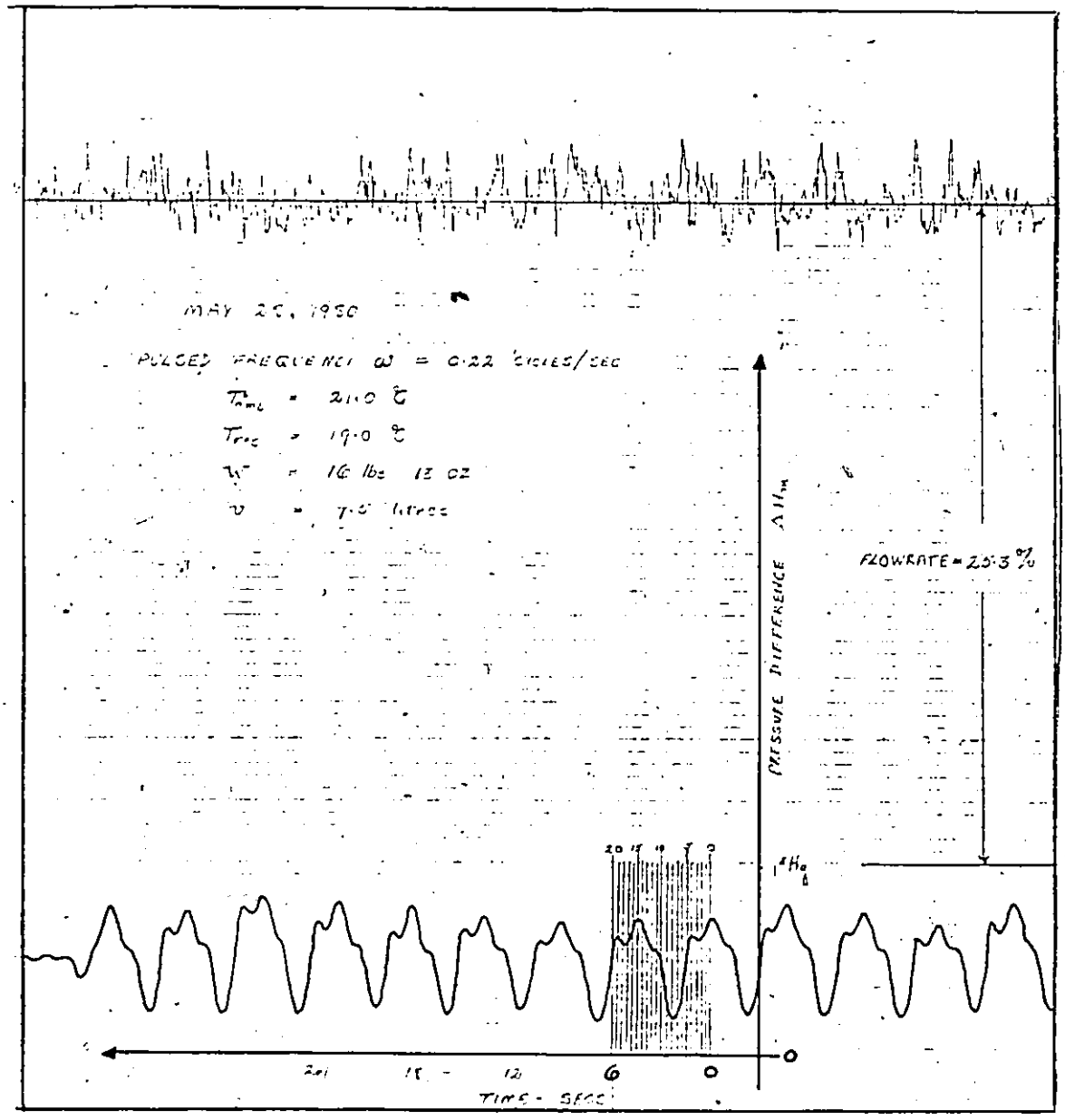

FIGURE (A-3). Sample Work Sheet and Pulsed-Flow Trace

Since Q = 25.3%,

then $\overline{V}_m = Q \times 0.055 = 1.39$ (m/s)

giving $\psi = (211.1) / \overline{V}_m = 152$

and $Re = \frac{1.39 \times (0.99843 \times 10^3) \times 0.051}{1.0299 \times 10^{-3}} = 68,724$

from Figure D-1, $f = 0.0272$

$$i_w = 0.0272 \times \frac{1}{0.051} \times \frac{(1.39)^2}{2 \times 9.81} = 0.052 \text{ (m of water/m)}$$

from Figure 6.12, at $\psi = 152$, $\phi = 6.6$

Hence $i = C_s \times i_w \times \phi + i_w$

$= 0.011 \times 0.052 \times 6.6 + 0.052$

$= 0.056$ (m of water/m)

then $J_s = 0.056 \left(\frac{0.99843}{1.0175}\right) + \left(\frac{0.99802}{1.0175}\right)$

$= 1.036$ (m of water/m)

and $J_p/J_s = \frac{1.060}{1.036} = 1.023$

at $\omega = \frac{1}{n\Delta t} = \frac{1}{15 \times 0.305} = 0.22$ cycles per second

APPENDIX B

CALIBRATION CURVES

I. Calibration of Flowmeter

Prior to data collection, measurement experiments were conducted in order to determine the 100% indicator flow rate on the Brooks-Mag Electromagnetic flowmeter. With the flow system and flowmeter prepared as described in sections 5.1 (a) and (b), steady flow was obtained at a fixed pump speed. The pump speed was checked with a stroboscope, and set using the adjustable motor base to change the effective motor sheave diameter. After stabilized flow was achieved and the flowmeter warmed up, the exit flow was discharged for a measured time into the 300 litre overflow tank. The initial and final depth H_i and H_f of the water collected in the tank, along with the flowmeter indicator reading were then recorded. These readings are tabulated in Table (B-1) while the calibration results are displayed in Figures (B-1) and (B-2). The results showed excellent agreement when compared with the characteristic curves given by the manufacturer.

TABLE (B-1)

Pump Speed (RPM)		Run I	Run II	Run III	Run IV	Flowmeter Indicated Reading %
	H_f (in)	6 1/8	12 1/2	10 13/16	16 1/2	
325	H_i (in)	0	6 1/8	4 9/16	10 13/16	21
	time (s)	49.20	49.90	50.10	50.10	
	H_f (in)	11 1/16	14 5/16	14 5/16	17 1/16	
500	H_i (in)	5 3/16	8 5/16	8 5/16	11 3/16	32
	time (s)	30.00	30.50	30.25	30.50	
	H_f (in)	7 7/8	13 5/16	11 1/16	16 15/16	
700	H_i (in)	2 3/16	7 7/8	4 11/16	11 1/16	46
	time (s)	20.80	21.50	23.20	21.30	
	H_f (in)	4 13/16	9 1/4	13 11/16	12 1/2	
910	H_i (in)	0	4 13/16	9 1/4	7 15/16	62
	time (s)	13.50	12.35	12.30	12.75	

FIG (B-1) : Graph to determine 100% maximum flow

Calculated Flow Rate (U.S. GPM) = $\frac{\text{(Hf-Hi) (in)}}{\text{12(in/ft)}} * \frac{\text{7.875 (sq ft)}}{\text{t (seconds)}} * \text{60 (sec./min)} * \text{7.488(cuft)}$

(BROOKS-MAG FLOWMETER MODEL 7100/7200)
(SER: 16906-27442/IE)
(OCT. 25, 1979)

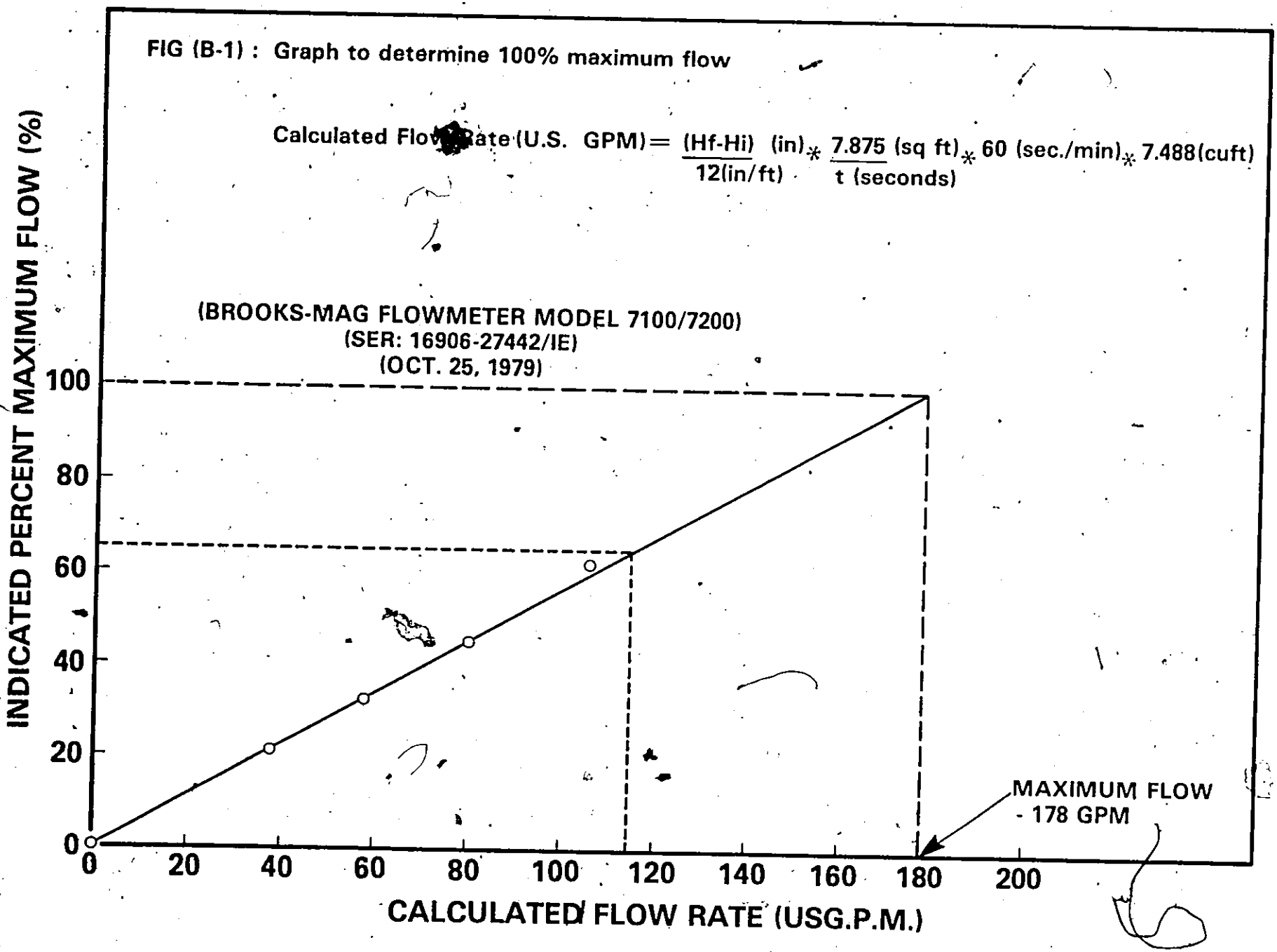

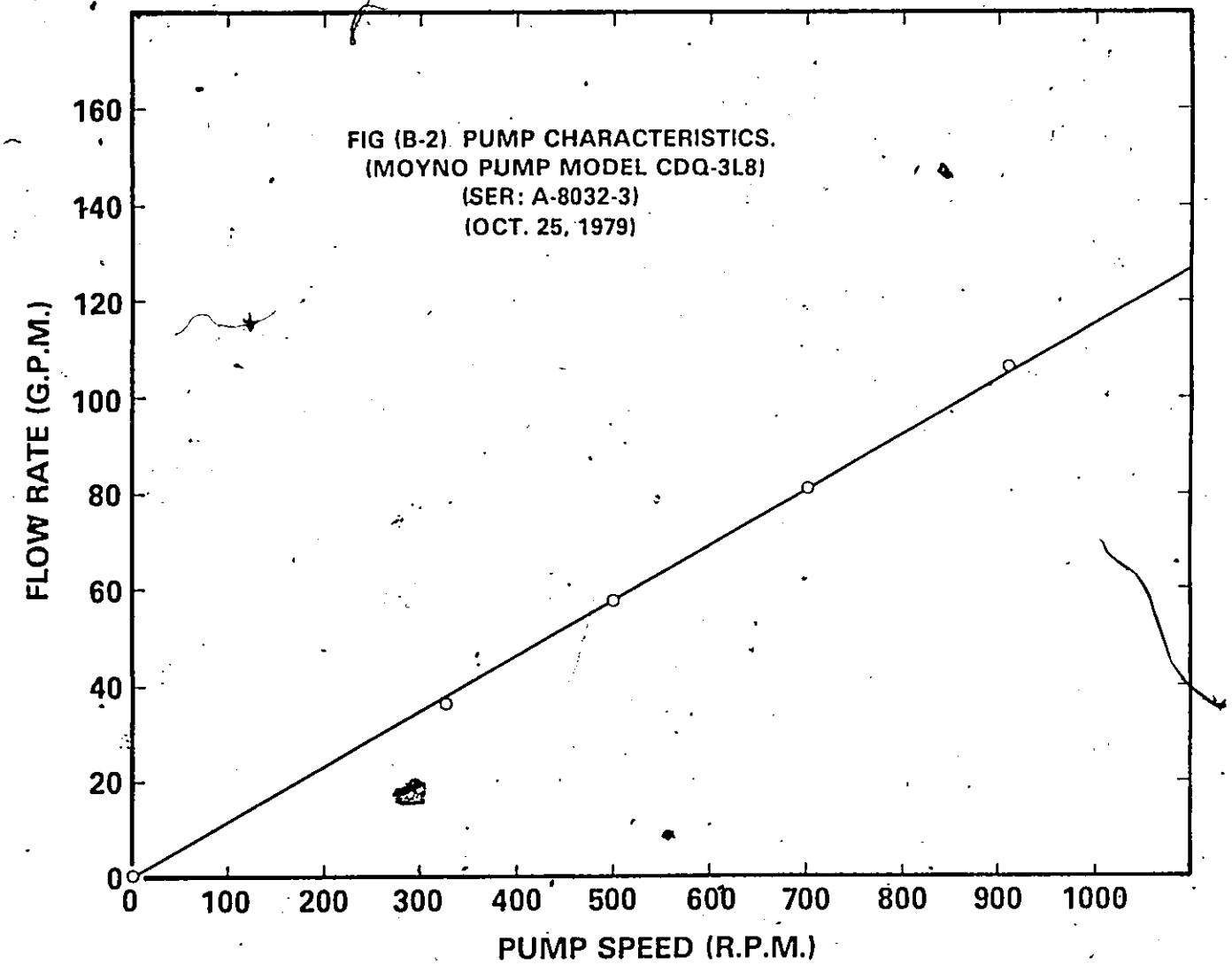
FIG (B-2) PUMP CHARACTERISTICS.
(MOYNO PUMP MODEL CDQ-3L8)
(SER: A-8032-3)
(OCT. 25, 1979)
FLOW RATE (G.P.M.)
0
20
40
60
80
100
120
140
160
0
100
200
300
400
500
600
700
800
900
1000
PUMP SPEED (R.P.M.)

II. Calibration of Pressure Transducer

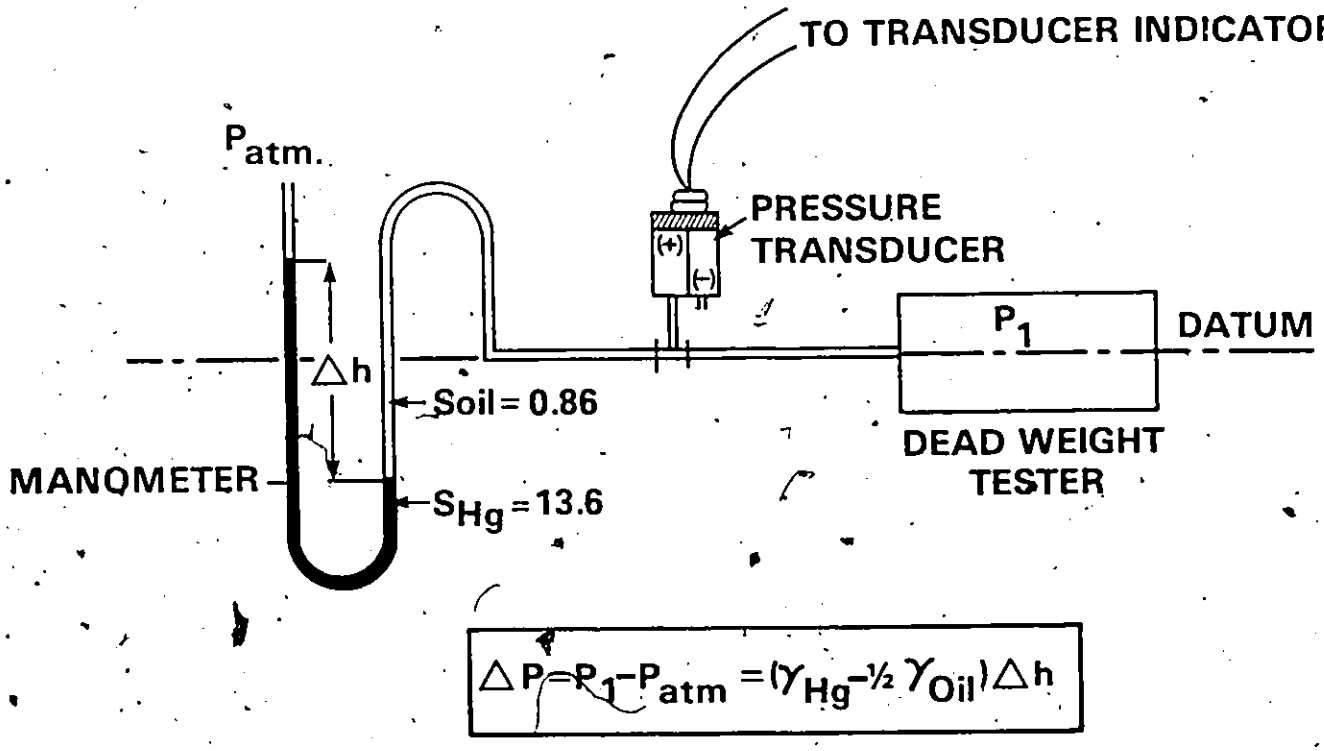

FIG. (B-3) CALIBRATION OF PRESSURE TRANSDUCER

The calibration of the pressure transducer which had a ± 5 psiD diaphragm was done using a dead-weight tester, a schematic of which is shown in Figure (B-3).

By varying the pressure inside the tester, a corresponding variation of the manometer fluid column and a direct pressure reading from the pressure transducer were obtained. The true pressures calculated from Equation (B-2) were plotted against the transducer reading to obtain the calibration curve Figure (B-4) of the transducer with the particular diaphragm.

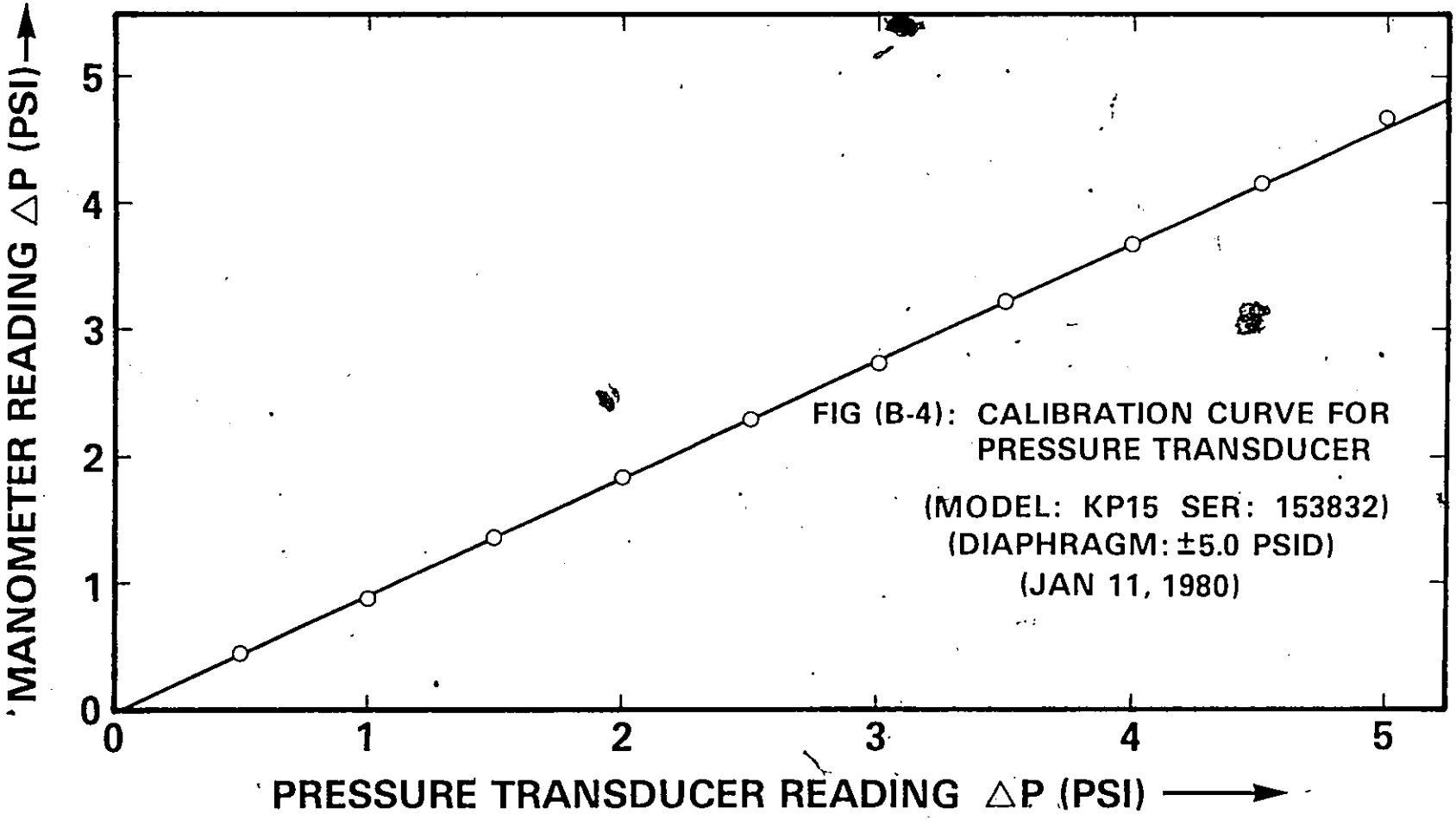

FIG (B-4): CALIBRATION CURVE FOR PRESSURE TRANSDUCER

(MODEL: KP15 SER: 153832)
(DIAPHRAGM: ±5.0 PSID)
(JAN 11, 1980)

APPENDIX C

THE VELOCITY PROFILE OF THE TEST SECTION

An extremely important condition, under which the experimental data at the test section can be considered acceptable, was that flow within the test section must be fully developed and symmetrical. In order to confirm this, the flow velocity profile just prior to the test section was determined by using the pitot-static tube transverse method.

The measured results are listed in Table (C-1) and the velocity profile is shown in Figure (C-1). The profile is accurately described by the following equation:

$$\frac{u}{U} = (y/R)^{1/9} \qquad \text{(C-1)}$$

The average percentage error obtained using equation (C-1) is + 2.0%.

TABLE C-1: Cross-Sectional Velocity Distribution of the Test Section

y/R	Pilot-tube Measurement h (cm. CCl4)	$u = 1.11\sqrt{h}$ (ft/sec)	u/U
0.22	15.9	4.43	0.88
0.31	16.0	4.45	0.88
0.37	16.7	4.54	0.90
0.50	16.9	4.57	0.91
0.62	19.1	4.86	0.97
0.78	19.5	4.91	0.98
1.00	20.5	5.03	1.00
1.19	19.5	4.91	0.98
1.31	18.3	4.75	0.94
1.44	16.0	4.45	0.88
1.56	14.7	4.26	0.85
1.75	12.1	3.87	0.77
1.97	8.5	3.24	0.64

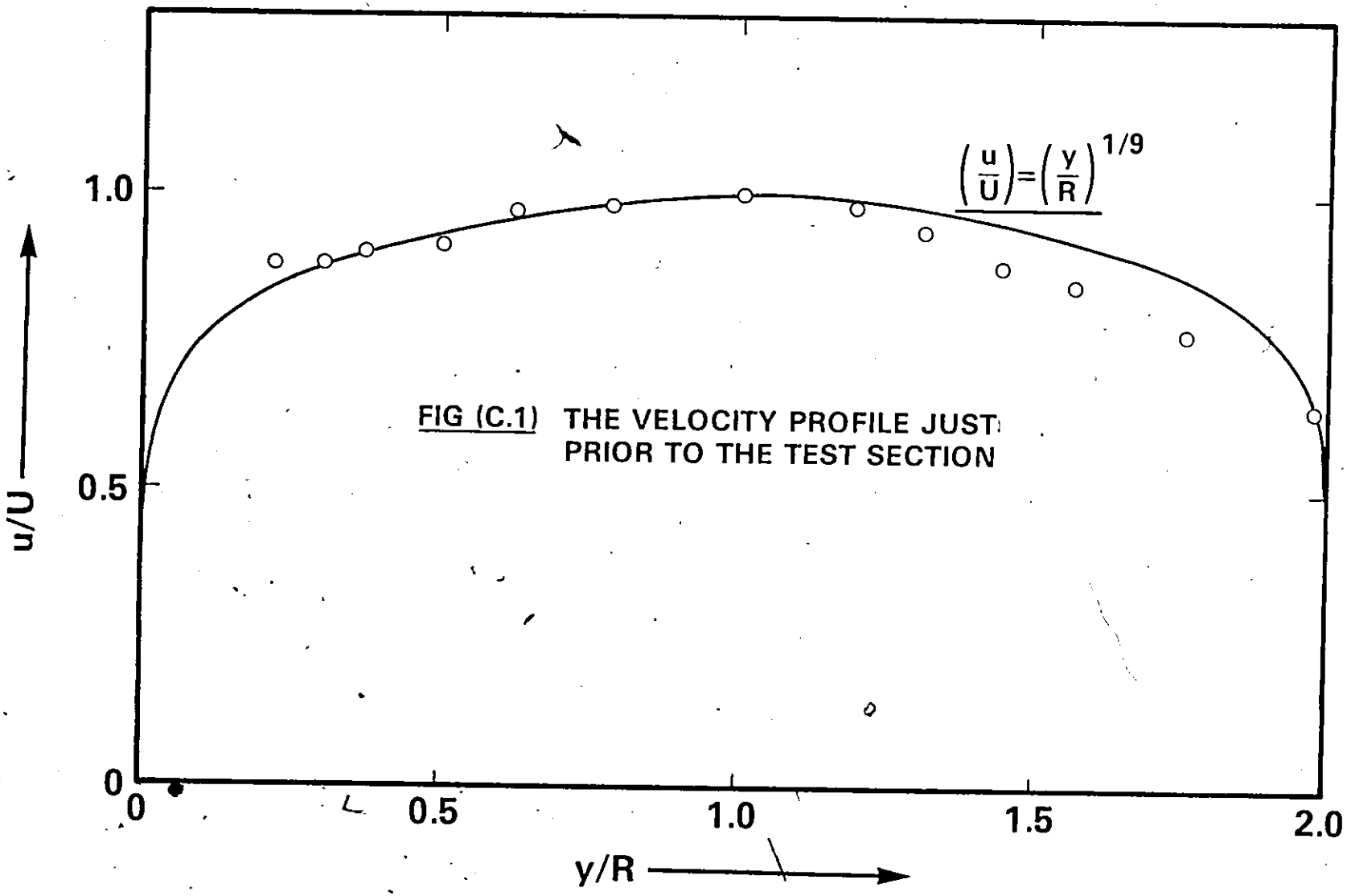

FIG (C.1) THE VELOCITY PROFILE JUST PRIOR TO THE TEST SECTION

APPENDIX D

VARIATION OF FRICTION FACTOR WITH REYNOLDS-NUMBER

The dissipation of energy by fluid friction results in a fall of specific pressure head in the direction of flow, and if the pipe is of uniform cross-section and roughness, and the flow is 'fully developed', the specific pressure head falls uniformly. The general equation for pressure drop, known as Darcy's formula and expressed in metres of fluid is:

$$h_L = \frac{\Delta P}{\rho g} = f \frac{\Delta Z}{D} \frac{\bar{u}^2}{2g} \qquad \text{(D-1)}$$

The coefficient f is usually known as the friction factor and is a function of Reynolds number and of the relative roughness. By plotting the friction factor at various Reynolds numbers using the Moody diagram, it was possible to determine the relative roughness of the test section and the flow region of the experiments. The flow velocity was determined using the pitot-static tube located at the point of maximum flow in the velocity profile. From the pitot tube measurements, the maximum flow velocity, U, and consequently the average flow velocity, $\bar{u}$ were obtained using the following relationships:

$$U = \sqrt{(S - 1)\ 2gh} \qquad \text{(D-2)}$$

where S = specific gravity of manometer liquid

h = height of liquid column in manometer

$$\frac{\bar{u}}{U} = \frac{2}{(n + 1)\ (n + 2)} \qquad \text{(D-3)}$$

where $$\frac{u}{U} = \left(\frac{y}{R}\right)^n$$

and $n = \frac{1}{9}$ (Appendix C)

The pressure drop across the test section was accurately determined using a mercury manometer fitted with a vernier reading to 0.001 in Hg. The calculation of the Reynolds number took into account the changes in viscosity and density with the change in water temperature. The results obtained are presented in Table (D-1) and Figure (D-1). The relative roughness and the actual roughness of the test section were found to be approximately 0.003 and 0.15 mm respectively.

TABLE (D-1)

Reservoir Temp. ^{o}C	ΔP (in Hg.)	h (cm ccl4) or (in Hg.)*	$\bar{u}$* (m/s)	Re x 10^{-4}	h_L (ft.H_2O)	f
11.0	0.149	7.6	0.79	3.20	0.047	0.0337
12.3	0.332	20.5	1.31	5.47	0.106	0.0279
13.0	0.594	34.9	1.71	7.24	0.190	0.0293
11.0	0.991	64.8	2.32	9.34	0.317	0.0263
14.2	1.102	1.245*	2.39	10.45	0.353	0.0278
16.0	1.355	1.644*	2.74	12.58	0.434	0.0259
17.7	1.697	2.153*	3.14	15.03	0.543	0.0248

* $\bar{u} = 0.853\ U$.

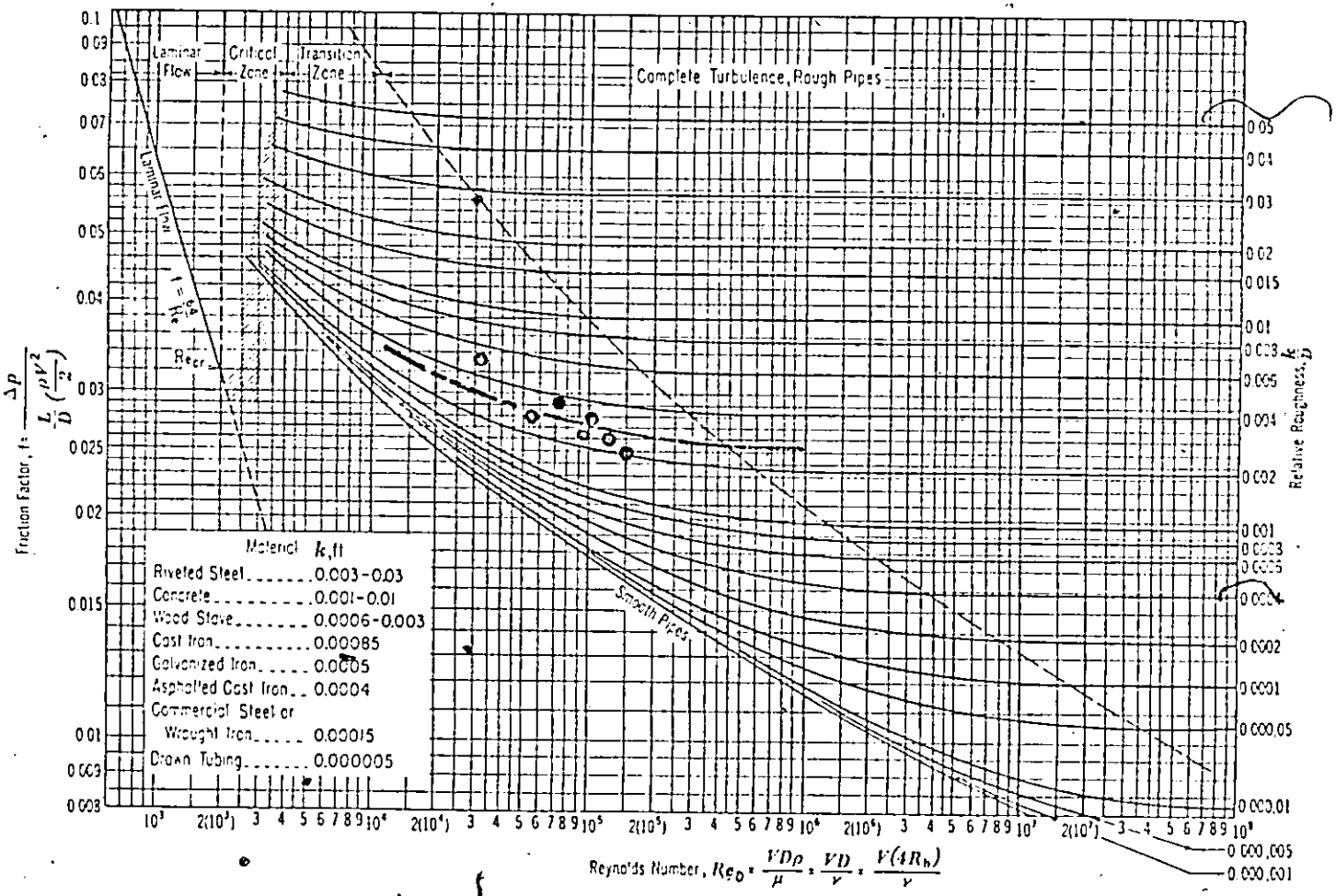

FIGURE (D-1). Variation of Friction Factor with Reynolds Number on the Moody Diagram

APPENDIX E

ERROR ANALYSIS

Listed in Table (E-1) are the estimates of relative uncertainty of the primary measurements made in the present work. They include factors such as instrument error, human error, calibration error and random error.

By using the "most probable" method, the relative error of each of the important variables used in this study are determined as follows:

For a given variable M, which is a function of x, y, ..., the relative error in M may be expressed by the equation:

$$\frac{dM}{M} = \left\{ \frac{1}{M^2} \left[\left(\frac{\delta M}{\delta x} \, dx \right)^2 + \left(\frac{\delta M}{\delta y} \, dy \right)^2 + \ldots \right] \right\}^{1/2}$$

$$\text{or} \qquad E_m = \left[(E_x)^2 + (E_y)^2 + \ldots \right]^{1/2} \qquad \text{(E-1)}$$

where E_x, E_y ... are the relative uncertainties in x, y, ...

(1) Error in $\overline{V}_m$

$$\text{Since } \overline{V}_m = \frac{4Q}{\pi D^2} = \text{Constant} \times \frac{Q}{D^2}$$

TABLE (E-1). Uncertainty Estimates in the Measured Primary Quantities

Description	Symbol	Uncertainty ± %
Pipe inside diameter	D	2.0
Gravel weighted average diameter	d	1.0
Length of test section	ΔZ	1.0
Flowrate measurements	Q	4.0
Manometer measurements	ΔH_m	1.0
Temperature	T	2.0
Weight of mixture sample	W	1.0
Volume of mixture sample	v	1.0
Viscosity	μ	2.0
Specific gravity of sand	S	0.5

$$\therefore \quad \frac{d\bar{V}_m}{\bar{V}_m} = \left\{\left(\frac{dQ}{Q}\right)^2 + 2\left(\frac{dD}{D}\right)^2\right\}^{1/2}$$

Hence, from Table (E-1), the relative error in $\bar{V}_m$ is

$$E_{\bar{V}_m} = [(E_Q)^2 + 2\ (E_D)^2]^{1/2} = [(4)^2 + 2\ (2)^2]^{1/2} \cong \pm 5.0\ \%$$

(2) Error in Re

Since $Re = \frac{\rho_{wr}\ \bar{V}_m\ D}{\mu_{wr}}$

$$\therefore \quad E_{Re} = [(E_\rho)^2 + (E_{\bar{V}_m})^2 + (E_D)^2 + (E_\mu)^2]^{1/2}$$

$$= [(0) + (5)^2 + (2)^2 + (2)^2]^{1/2} \cong \pm 5.5\ \%$$

(3) Error in ρ_m

Since $\rho_m = \frac{W}{v} \times \text{constant}$

$$\therefore \quad E_{\rho_m} = [(E_w)^2 + (E_v)^2]$$

$$= [(1)^2 + (1)^2]^{1/2} \cong \pm 1.5\ \%$$

(4) Error in i

$$\text{Since } i \simeq \frac{\Delta H_m}{\Delta Z}\left(\frac{\rho_{HG}}{\rho_{wr}} - 1\right).$$

$$\simeq \text{constant} \times \frac{\Delta H_m}{\Delta Z}$$

$$E_i = \left[(E_{\Delta H_m})^2 + (E_{\Delta Z})^2\right]^{1/2}$$

$$= \left[(1)^2 + (1)^2\right]^{1/2} \simeq \pm 1.5\ \%$$

(5) Error in C_s

Since $C_s = \left[\left(\rho_{mr}/\rho_{wr}\right) - 1\right] / (S - 1)$, the relative error in C_s cannot be calculated strictly from the method used so far. Firstly, the actual uncertainties of the terms $\left(\frac{\rho_{mr}}{\rho_{wr}} - 1\right)$ and $(S - 1)$ must be estimated. It will be noticed that the relative error in C_s depends almost entirely on its absolute value. Thus, at $C_s = 0.05$, $\rho_m/\rho_w \simeq 1.08 \pm 0.01$, and $s \simeq 2.6 \pm 0.01$.

Giving, $$E_{C_s} = \left\{\left[E_{(\rho_m/\rho_w - 1)}\right]^2 + \left[E_{(S-1)}\right]^2\right\}^{1/2}$$

$$= \left[(12.5)^2 + (0.6)^2\right]^{1/2} \simeq \pm 12.5\ \%$$

At $C_s = 0.10$ $\quad E_{C_s} \simeq \pm 6.0\ \%$

At $C_s = 0.20$ $\quad E_{C_s} \simeq \pm 3.0\ \%$

(6) Error in J_p/J_s

Since J_p was calculated from Eq. (A-13), the relative error in J_p may be considered due to the error in $\bar{i}_T$ and ρ_{mr} only.

$$\text{Giving, } E_{J_p} = \left[(E_i)^2 + (E_{\rho_{mr}})^2\right]^{1/2}$$

$$= \left[(1.5)^2 + (1)^2\right]^2 \simeq \pm 2.0\ \%$$

J_s was calculated from Eq. (A-10). In this case, however, the value of i was calculated using Figure (6.12). Therefore the relative error in J_s may be considered due to the error in C_s and ρ_{mr}.

$$\text{Giving, } E_{J_s} = \left[(E_{C_s})^2 + (E_{\rho_{mr}})^2\right]^{1/2}$$

$$= \left[(10.0)^2 + (2)^2\right]^{1/2} \simeq \pm 10.0\ \%$$

$$\text{and Error in } J_p/J_s = \left[(E_{J_p})^2 + (E_{J_s})^2\right]^{1/2} \simeq \pm 10.0\ \%$$

These estimates of accuracy of the primary functions are listed in Table (E-2) and appear to be within acceptable limits.

TABLE (E-2). Estimate of Accuracy of the Primary Functions

Description	Symbol	Uncertainty %
Average mixture velocity	$\overline{V}_m$	5.0
Reynolds number	Re	5.5
Mixture density	ρ_m	1.0
Pressure gradient	i	1.5
Delivered volumetric concentration	C_s	
at 5.0 %		12.5
at 20.0 %		3.0
Energy ratio	J_p/J_s	10.0

APPENDIX F

TABLES OF EXPERIMENTAL DATA AND CALCULATED RESULTS

TABLE (F-1). Experimental Data For Steady Flow of Sand-A Slurries

Data Point Number	ΔHm (in. Hg)	Q (%)	T_{amb} (^{o}C)	T_{res} (^{o}C)	W (lb-oz)	v (litres)
101	0.501	15.0	19.5	21.0	15-13	6.45
102	0.699	38.0	20.0	8.0	24-3	10.35
103	1.377	40.0	23.0	10.0	21-5	8.48
104	1.289	28.0	20.0	10.0	23-12	9.55
105	0.835	38.0	21.0	6.0	23-2	9.86
106	0.545	27.0	20.0	7.0	20-4	8.94
107	0.500	19.0	22.0	7.5	20-10	8.88
108	1.837	32.0	21.0	7.0	25-0	9.44
109	2.167	32.0	20.0	7.0	24-8	8.77
110	2.507	40.0	18.5	7.5	30-1	10.39
111	2.884	46.0	19.0	8.0	30-12	10.15
112	0.988	38.0	22.0	7.0	19-7	8.00
113	0.734	35.0	21.0	7.0	21-2	8.94
114	0.729	30.0	21.0	9.5	21-8	9.40
115	0.516	21.0	21.5	6.0	20-1	8.68
116	1.037	44.0	22.0	7.5	23-13	10.51
117	1.290	48.0	20.5	7.5	20-15	8.81
118	1.583	44.0	19.5	7.0	21-11	8.88
119	2.050	50.0	21.0	10.0	26-5	10.00
120	2.348	38.0	20.5	10.5	26-3	9.53
121	2.696	40.0	21.0	13.5	25-4	8.95
122	3.184	50.0	20.5	12.0	29-4	9.57
123	0.764	22.0	21.0	17.0	19-12	8.30
124	2.608	48.0	22.5	20.5	27-4	9.84
125	2.381	36.0	20.5	12.0	28-2	10.58
126	2.221	32.0	22.5	12.0	25-8	9.37
127	2.090	23.0	20.0	10.0	23-10	8.70
128	0.695	22.0	22.0	9.0	22-1	9.45

TABLE (F-2). Experimental Data for Steady Flow of Sand-B Slurries

Data Point Number	ΔHm (in.Hg)	Q (%)	T_{amb} (^{o}C)	T_{res} (^{o}C)	W (lb-oz)	v (litres)
201	0.263	17.7	20.3	19.2	25-8	11.48
202	0.396	26.4	21.0	21.0	30-1	13.49
203	0.294	17.5	20.7	21.0	27-8	12.22
204	0.400	24.6	20.6	22.2	32-1	14.08
205	0.500	33.9	20.7	24.0	26-8	11.69
206	0.341	17.5	20.0	23.2	26-14	11.90
207	0.429	20.6	20.0	24.4	27-14	12.11
208	0.447	16.9	21.0	22.0	23-8	10.32
209	0.565	22.8	20.4	24.3	26-1	10.51
210	0.517	25.3	21.0	17.0	17-11½	7.90
211	0.563	25.8	21.0	16.8	41-6½	18.22
212	0.602	25.7	21.0	19.2	28-9	12.34
213	0.610	22.6	21.0	15.5	29-7	12.45

TABLE (F-3). Experimental Data for Steady Flow of Sand-C Slurries

Data Point Number	ΔHm (in.Hg)	Q (%)	T_{amb} (^{o}C)	T_{res} (^{o}C)	W (lb-oz)	v (litres)
301	0.577	24.6	21.0	17.5	28-13	12.45
302	0.712	29.5	21.5	19.3	33-5	14.43
303	0.756	37.0	20.8	21.3	39-5	17.00
304	0.773	42.1	21.1	24.8	33-5	14.16
305	0.341	17.3	22.0	22.0	27-13	12.34
306	0.461	16.8	22.0	23.0	33-15	14.69
307	0.587	19.1	22.2	24.2	36-14	15.95
308	0.760	24.1	22.0	26.0	36-0	15.72
309	0.760	28.7	22.6	28.1	32-9	13.59
310	0.405	17.1	22.0	21.7	31-14	14.08
311	0.622	21.7	22.8	23.0	38-2	16.30
312	0.762	24.9	22.5	24.0	37-14	16.01
313	0.961	30.4	22.5	26.0	32-4	13.65
314	0.289	18.2	21.3	19.5	32-6	14.16
315	0.358	21.8	22.4	21.0	35-5	15.72
316	0.458	25.8	22.5	22.0	32-0	14.08
317	0.509	31.6	22.0	24.0	32-7	14.43

TABLE (F-4). Experimental Data for Steady Flow of Lime Slurries

Data Point Number	ΔHm (in.Hg)	Q (%)	T_{amb} (°C)	T_{res} (°C)	C_m
401	1.897	31.8	24.0	24.0	0.072
402	1.543	16.2	23.0	24.5	0.072
403	1.778	27.5	23.5	25.0	0.072
404	2.168	41.2	24.0	26.0	0.072
405	2.556	50.7	24.0	27.0	0.072
406	2.766	59.3	24.0	29.0	0.072
407	2.610	50.5	24.0	31.0	0.098
408	2.882	58.0	25.0	34.0	0.098
409	2.094	40.7	24.5	32.0	0.098
410	1.794	30.0	25.2	34.0	0.098
411	1.701	25.0	25.5	33.0	0.098
412	2.173	41.8	23.0	26.2	0.098
413	2.036	41.8	23.0	26.0	0.077
414	1.825	34.4	23.0	27.0	0.074
415	1.736	29.2	23.5	27.5	0.076
416	1.645	24.0	23.3	28.0	0.076
417	2.323	51.7	24.2	29.2	0.077
418	2.093	51.7	24.2	30.0	0.049
419	1.781	40.2	24.5	30.2	0.050
420	1.624	34.4	24.0	31.0	0.048
421	1.465	28.8	24.0	31.0	0.051
422	1.390	17.2	24.2	31.0	0.048

TABLE (F-5). Flow Conditions of Sand-A Slurries

Data Point Number	C_s	$\overline{V}_m$ (m/s)	i mH_2O/m	Re	i_w mH_2O/m
101	0.07	0.82	0.072	42,545	0.019
102	0.04	2.09	0.098	76,828	0.118
103	0.09	2.20	0.195	85,580	0.130
104	0.08	1.54	0.183	60,060	0.065
105	0.04	2.09	0.118	72,372	0.119
106	0.02	1.48	0.076	52,842	0.061
107	0.03	1.04	0.070	37,692	0.030
108	0.12	1.76	0.262	62,839	0.085
109	0.16	1.76	0.309	62,839	0.085
110	0.19	2.20	0.359	79,733	0.130
111	0.23	2.53	0.412	93,095	0.171
112	0.06	2.09	0.140	74,622	0.118
113	0.04	1.92	0.103	68,552	0.100
114	0.02	1.65	0.103	63,418	0.075
115	0.03	1.15	0.072	39,822	0.038
116	0.02	2.42	0.147	87,706	0.157
117	0.05	2.64	0.183	95,679	0.184
118	0.07	2.42	0.225	86,404	0.157
119	0.12	2.75	0.296	101,249	0.200
120	0.15	2.09	0.335	82,660	0.117
121	0.17	2.20	0.388	94,540	0.129
122	0.24	2.75	0.456	113,443	0.199
123	0.05	1.21	0.109	56,991	0.041
124	0.16	2.64	0.375	122,478	0.182
125	0.13	1.98	0.341	81,679	0.105
126	0.15	1.76	0.318	72,604	0.084
127	0.14	1.26	0.298	49,140	0.045
128	0.04	1.21	0.099	45,840	0.042

TABLE (F-6). Flow Conditions of Sand-B Slurries

Data Point Number	C_s	$\overline{V}_m$ (m/s)	i mH_2O/m	Re	i_w mH_2O/m
201	0.01	0.97	0.038	48,171	0.026
202	0.01	1.45	0.057	75,231	0.057
203	0.01	0.96	0.042	49,808	0.026
204	0.02	1.35	0.057	72,063	0.049
205	0.02	1.86	0.073	103,451	0.092
206	0.02	0.96	0.050	52,430	0.026
207	0.03	1.13	0.063	63,418	0.035
208	0.02	0.93	0.064	49,415	0.024
209	0.08	1.25	0.082	70,000	0.043
210	0.01	1.39	0.073	65,403	0.053
211	0.02	1.42	0.080	66,465	0.055
212	0.03	1.41	0.086	70,023	0.054
213	0.04	1.24	0.087	56,122	0.043

TABLE (F-7). Flow Conditions of Sand-C Slurries

Data Point Number	C_s	$\overline{V}_m$ (m/s)	i mH_2O/m	Re	i_w mH_2O/m
301	0.03	1.35	0.082	64,323	0.050
302	0.03	1.62	0.102	80,648	0.071
303	0.03	2.03	0.109	106,070	0.109
304	0.04	2.31	0.112	130,827	0.139
305	0.01	0.95	0.049	50,478	0.025
306	0.03	0.92	0.067	49,988	0.024
307	0.03	1.05	0.085	58,663	0.029
308	0.03	1.32	0.110	76,820	0.047
309	0.06	1.58	0.111	96,209	0.066
310	0.02	0.94	0.058	49,590	0.025
311	0.04	1.19	0.090	64,659	0.039
312	0.05	1.37	0.110	76,198	0.051
313	0.05	1.67	0.139	97,178	0.074
314	0.02	1.00	0.041	50,027	0.028
315	0.01	1.20	0.051	62,260	0.040
316	0.02	1.42	0.066	75,452	0.054
317	0.01	1.74	0.074	96,777	0.081

TABLE (F-8). Flow Conditions of Lime Slurries

Data Point Number	C_s	$\overline{V}_m$ (m/s)	i (mH_2O/m)	Re	i_w (mH_2O/m)
401	0.032	1.75	0.272	97,333	0.081
402	0.032	0.89	0.222	50,065	0.022
403	0.032	1.51	0.255	85,911	0.061
404	0.032	2.27	0.311	132,108	0.134
405	0.032	2.79	0.366	165,852	0.201
406	0.032	3.26	0.398	204,068	0.270
407	0.042	2.78	0.377	179,938	0.198
408	0.042	3.19	0.417	219,613	0.257
409	0.042	2.24	0.303	148,025	0.130
410	0.042	1.65	0.261	113,479	0.071
411	0.042	1.37	0.246	92,411	0.050
412	0.042	2.30	0.312	134,438	0.137
413	0.034	2.30	0.292	133,854	0.137
414	0.033	1.89	0.263	112,351	0.094
415	0.034	1.61	0.250	96,760	0.069
416	0.034	1.32	0.237	80,204	0.047
417	0.034	2.84	0.335	177,115	0.207
418	0.021	2.84	0.302	180,168	0.207
419	0.022	2.21	0.257	140,324	0.127
420	0.021	1.89	0.235	122,332	0.093
421	0.022	1.58	0.212	102,267	0.066
422	0.021	0.95	0.202	61,489	0.025

TABLE (F-9). Experimental Data for Pulsating Flow of Sand-B Slurries at 0.22 Cycles per Second

Data Point Number	$\overline{\Sigma H}_{mj}$ (m.Hg.)	Q	T_{amb} (^{o}C)	T_{res} (^{o}C)	W (lb-oz)	v (litres)
501	7.72	25.3	21.0	18.0	19-10½	8.7
502	8.451	25.3	21.0	19.0	16-13	7.5
503	8.150	25.3	21.0	19.0	16-13	7.5
504	11.004	25.7	21.0	18.0	31-11.5	13.84
505	8.781	25.7	21.0	18.5	26-15.5	11.79
506	12.157	23.5	21.0	20.5	31-5	12.91
507	12.194	22.6	21.0	21.5	28-4	12.00

TABLE (F-10). Pulsed Flow Condition of Sand-B Slurries at 0.22 Cycles per Second

Data Point Number	C_s	$\overline{V}_m$ (m/s)	$\overline{i}_T$ (mH_2O/m)	Re	J_p/J_s
501	0.016	1.39	1.100	67,044	1.01
502	0.011	1.39	1.208	68,724	1.02
503	0.011	1.39	1.165	68,724	1.02
504	0.025	1.41	1.572	68,009	1.04
505	0.024	1.41	1.254	68,850	1.02
506	0.062	1.29	1.745	66,130	1.04
507	0.043	1.24	1.754	65,128	1.05

REFERENCES

Baird, M. H. I.; Senior, M. G.; Thompson, R. J.: "Terminal velocities of spherical particles in a vertically oscillating liquid", Chem. Eng. Sci., 22, pp. 551-558 (1967).

Barton, P.; Fenske, M. R.: "Hydrocarbon extraction of saline waters", Ind. Eng. Chem., Process, Design & Dev., 9, pp. 18 (1970).

Basset, A. B.: "On the motion of a sphere in a viscous liquid", Philos, Trans. Roy. Soc. London, Ser. A, 179, pp. 43-63 (1888).

Bhattacharya, A.; Roy, A. N.: "Flow of solid-liquid suspensions in vertical columns", Ind. Eng. Chem., 47, pp. 268-274 (1955).

Brodkey, R. S.: "The phenomena of fluid motions", Addison-Wesley Publishing Co. (1967).

Carstens, M. R.; Roller, J. E.: "Boundary-shear stress in unsteady turbulent pipe flow", ASCE Proceedings, Journal of the Hydraulic Division, Vol. 85, Part I (1959).

Chonowski, A.; Angelino, H.: "Étude en régime non laminaire mouvement d'une goutte dans un milieu pulsé", Can. J. Chem. Eng., 50, pp. 23 (1972).

Cloete, F. L. D.; Miller, A. I.; Streat, M.: "Dense phase flow of solids-water mixtures through vertical pipes", Trans. Instn. Chem. Engrs, 45, pp. T392-T400 (1967).

Colamussi, A.; Merli, V.: "Transport of solids by water: study of pulsating systems", Dock and Harbour Authority, pp. 479-482 (1972).

Durand, R.: "Ecoulements de mixture en conduites verticales", La Houille Blanche, pp. 124-129 (1953).

Edwards, M. F.; Wilkinson, W. L.: "Review of potential applications of pulsating flow in pipes", Trans. Inst. Chem. Engrs., 49, pp. 85-94 (1971).

Field, W. G.: "Effects of density ratio on sedimentary similitude", J. Hydraulics Div. ASCE, 94 (HY6) (1968).

Frantz, J. F.: "Design for fluidization", Chem. Eng., 69 (Sept. 17), 161; 69 (Oct. 1), 89; 69 (Oct. 29), 103 (1962).

Govier, G. W.; Aziz, K.: "The flow of complex mixtures in pipes", Van Nostrand Reinhold Co. (1972).

Harzer, H.; "Hydraulic hoisting in the mining industry of the Federal Republic of Germany", Paper A2, Hydrotransport 3, (May 17) (1974).

Herringe, R. A.: "On the motion of small spheres in oscillating liquids", Chem. Eng. J., 11, pp. 89-99 (1976).

Hjelmfelt, A. T.; Mockros, L. F.: "Motion of discrete particles in a turbulent fluid", Appl. Sci. Res., 16, pp. 149-161 (1966).

Ho, H. W., Ph.D. Thesis, State University Iowa, Univ. Microfilms, Ann Arbor, Michigan (1964) from Herringe (1976).

Houghton, G.: "The behaviour of particles in a sinusoidal velocity field", Proc. Roy. Soc. Ser. A, 272, pp. 33-43 (1963).

Houghton, G.: "Particle trajectories and terminal velocities in vertically oscillating fluids", Can. J. Chem. Eng., 44, pp. 90-95 (1966).

Houghton, G.: "Particle retardation in vertically oscillating fluids", Can. J. Chem. Eng., 46, pp. 79-81 (1968).

Kopko, R. J.; Barton, P.; McCormick, R. H.: "Hydrodynamics of vertical liquid-solids transport", Ind. Eng. Chem., Process Des. Dev., 14 No. 3, pp. 264-269 (1975).

Kostuik, S. P.: "Hydraulic hoisting and pilot-plant investigation of the pipeline transport of crushed magnetite", Trans. Can. Inst. Mining Met., 69, pp. 1 (1966).

McLachlan, N. W.: "Bessel functions for engineers", London: Oxford University Press (1941).

Molinier, J.; Angelino, H.: "De l'influence de la pulsation sur le temps de contact goutte-liquide", Can. J. Chem. Eng., 54, pp. 620-622 (1976).

Newitt, D. M.; Richardson, J. F.; Gliddon, B. J.: "Hydraulic conveying of solids in vertical pipes", Trans. Instn. Chem. Engrs, 39, pp. 93-100 (1961).

Oedjoe, D.; Buchanan, R. H.: "The pressure drop in the hydraulic lifting of dense slurries of large solids with wide size distribution", Trans. Instn. Chem. Engrs, 44 pp. T364 (1966).

Round, G. F.: "Pulsating flows-applications to the pipeline flow of solid-liquid suspensions", Paper B3, Hydrotransport 3 (1974).

Round, G. F.; Latto, B.; Lau, K-Y.: "Pulsating flows of solid-liquid suspensions", Paper D1, Hydrotransport 4 (1976).

Schlichting, H.: "Boundary layer theory", McGraw-Hill, New York (1968).

Shizgal, B.; Goldsmith, H. L.; Mason, S. G.: "The flow of suspensions through tubes IV: Oscillating flows of rigid spheres", Can. J. Chem. Eng., 43, pp. 47 (1965).

Tchen, C. M.: "Mean values and correlation problems connected with the motion of small particles suspended in a turbulent fluid", Ph.D. Thesis, Delft (1947).

Toda, M.; Konno, H.; Saito, S.; Maeda, S.: "Hydraulic conveying of solids through horizontal and vertical pipes", Int. Chem. Eng., 9, No. 3, pp. 553 (1969).

Tunstall, E. B.; Houghton, G.: "Retardation of falling spheres by hydrodynamic oscillations", Chem. Eng. Sci., 23, pp. 1067-1081 (1968).

Womersley, J. R.: "Method for the calculation of velocity, rate of flow and viscous drag in arteries when the pressure gradient is unknown", J. Physiol., 127, pp. 553-565 (1955).